Universiteit Antwerpen

This item is the archived peer-reviewed author-version of:

Spectroscopic investigations, DFT calculations, molecular docking and MD simulations of 3-[(4-Carboxyphenyl) carbamoyl]-4-hydroxy-2-oxo-1, 2-dihydroxy quinoline-6-carboxylic acid

Reference:
Ranjith P.K., Ignatious Angel, Panicker C. Yohannan, Sureshkumar B., Armakovic Stevan, Armakovic Sanja J., Van Alsenoy Christian, Anto P.L..-Spectroscopic investigations, DFT calculations, molecular docking and MD simulations of 3-[(4-Carboxyphenyl) carbamoyl]-4-hydroxy-2-oxo-1, 2-dihydroxy quinoline-6-carboxylic acid
Journal of molecular structure - ISSN 1872-8014 - 1264(2022), 133315
Full text (Publisher's DOI): https://doi.org/10.1016/J.MOLSTRUC.2022.133315
To cite this reference: https://hdl.handle.net/10067/1890710151162165141

uantwerpen.be
Institutional repository IRUA

Spectroscopic investigations, DFT calculations, molecular docking and MD simulations of 3-[(4-Carboxyphenyl) carbamoyl]-4-hydroxy-2-oxo-1, 2-dihydroxy quinoline-6-carboxylic acid.

P. K. Ranjith[a,b], Angel Ignatious[c], C. Yohannan Panicker[d], B. Sureshkumar[e], Stevan Armakovic[f], Sanja J. Armakovic[g], C. Van Alsenoy[h], P. L. Anto[a,c]*

[a] Department of Physics, Christ College (Autonomous), Irinjalakuda, Thrissur, Kerala, India

[b] Department of Physics, MPMMSN Trusts College, Shoranur, Palakkad, Kerala, India

[c] Department of Physics, St. Joseph's College (Autonomous), Irinjalakuda, Thrissur, Kerala, India

[d] Thushara, Neethinagar-64, Kollam, Kerala, India.

[e] Department of Chemistry, Sree Narayana College, Kollam, Kerala, India

[f] University of Novi Sad, Faculty of Sciences, Department of Physics, Trg D. Obradovica 4, 21000 Novi Sad, Serbia

[g] University of Novi Sad, Faculty of Sciences, Department of Chemistry, Biochemistry and Environmental Protection, Trg D. Obradovica 3, 21000 Novi Sad, Serbia

[h] Department of Chemistry, University of Antwerp, Groenenborgerlaan 171, B-2020, Antwerp, Belgium

* Corresponding author: email address: antoponnore367@gmail.com (P. L. Anto)

Abstract

In this article, the synthesis, experimental vibrational spectroscopic analysis (FT-IR and FT-Raman) and theoretical calculations of Quiniline derivative 3-[(4-Carboxyphenyl) carbamoyl]-4-hydroxy-2-oxo-1, 2-dihydroxy quinoline-6-carboxylic acid (CPCHODQ6C) were studied. The investigation of the IR and Raman spectra of the molecule under study, supported by DFT calculations, has afforded the opportunity to characterize explicitly the main vibrational bands for the title molecule, which is primarily used as anti-malaria compound. Computational calculations were done using B3LYP/6-31G(d) basis set. Vibrational assignments of

wavenumbers were performed on the basis of potential energy distribution. The downshift from the DFT value and the splitting of N-H stretching mode indicates the weakening of the N-H bond. Donor acceptor interactions were evaluated using NBO analysis. The change in polarizability values with halogen substitutions were calculated. The variations of HOMO-LUMO energy values and chemical descriptors with halogen substitutions were investigated. To foresee the important reactive sites of the title compound, we combined DFT calculations and molecular dynamics (MD) and visualized the ALIE and Fukui functions. Sensitive nature of the compound towards autoxidation and degradation in the presence of water was investigated by the calculation of BDE and RDF. By molecular docking study the compound forms a stable complex with ubiquinol-cytochrome–c reductase inhibitor.

Keywords: Quinoline, DFT, ALIE, RDF, BDE, Molecular Docking

1. Introduction

Quinoline derivatives possess number of medicinal properties like anti-bacterial [1] anti-filarial [2] anti-malarial [3,4] anti-fungal [5] cardiovascular [1] anti-tuberculosis [6]. 8-hydroxy quinoline derivative can be used as an active compound of pharmaceutical products [7] nuclear medicine [8] treating cancer [1] and neurodegeneration disorder [9]. Recent years DFT, molecular docking and vibrational studies of quinoline derivatives are reported [10]. Some quinoline derivatives are used as lifesaving drugs and have many applications like optical switches sensors in electro chemistry and in the area of inorganic chemistry [11,12]. Amino quinoline derivatives are a good candidate for the inhibition of human immuno virus (HIV) [13]. In order to analyse the effect of halogen substitution, in the parent molecule the hydrogen atoms 7H, 8H and 9H are replaced by fluorine, chlorine and bromine atoms which are designated as 7F, 8F, 9F for fluorine, 7Cl, 8Cl, 9Cl for chlorine and 7Br, 8Br, 9Br for bromine, respectively. Here we have spectroscopically characterized the title compound by employing FT-IR and FT-Raman techniques and to predict the local as well as global reactive properties by DFT calculations and MD simulations. Using DFT calculations we have also calculated the Frontier molecular orbitals (FMO) which helps us in understanding the HOMO-LUMO gap which determines the stability, hardness and many other parameters. To foresee about the reactive sites ALIE, MEP and Fukui function values are plotted against to the electron density surface. Thus, we can evaluate the prone sites of electrophilic and nucleophilic attacks. Organic

molecules with considerable biological activity and high stability are usually a threat to the nature [14]. Autoxidation and hydrolysis are important parameters that helps to analyse the degradation properties of the molecule. BDE (Bond dissociation energy) and RDF (Radial distribution functions) reflect the sensitivity of compounds towards the water environments, BDE and RDF can be evaluated using the MD simulations and DFT calculations. The greatest challenge in the production of pharmaceutical products is to find an active component, if the active component doesn't meet the requirements, it can be modified using an excipient. Using solubility parameter, we can easily find out an excipient [15–17]. Therefore, the aim of our study was to calculate and understand the degradation properties of target molecule, to check a suitable excipient and to perform molecular docking.

2. Experimental Details

3-[(4-Carboxyphenyl)carbamoyl]-4-hydroxy-2-oxo-1,2-dihydroquinoline-6-carboxylic acid was prepared by a microwave-assisted reaction of 4-aminobenzoic acid with triethyl methanetricarboxylate [18] (Scheme 1). All reagents were purchased from Aldrich. Kieselgel 60, 0.040-0.063 mm (Merck, Darmstadt, Germany) was used for column chromatography. TLC experiments were performed on alumina-backed silica gel 40 F254 plates (Merck). The plates were illuminated under UV (254 nm) and evaluated in iodine vapour. The melting points were determined on Boetius PHMK 05 (VEB Kombinat Nagema, Radebeul, Germany) and are uncorrected. Elemental analyses were carried out on an automatic Perkin-Elmer 240 microanalyser (Boston, USA). The purity of the final compounds was checked by the HPLC separation module Waters Alliance 2695 XE (Waters Corp., Milford, MA, USA). The detection wavelength 210 nm was chosen. The peaks in the chromatogram of the solvent (blank) were deducted from the peaks in the chromatogram of the sample solution. The purity of individual compounds was determined from the area peaks in the chromatogram of the sample solution. UV spectra (λ, nm) were determined on a Waters Photodiode Array Detector 2996 (Waters Corp.) in ca 6×10^{-4} mol methanolic solution and log ε (the logarithm of molar absorption coefficient ε) was calculated for the absolute maximum λ_{max} of individual target compounds. All ^{1}H NMR spectra were recorded on a Bruker AM-500 (499.95 MHz for ^{1}H), Bruker Bio Spin Corp., Germany. Chemicals shifts are reported in ppm (δ) to internal $Si(CH_3)_4$, when diffused easily exchangeable signals are omitted.

2.1 3-[(4-Carboxyphenyl) carbamoyl]-4-hydroxy-2-oxo-1, 2-dihydroxy quinoline-6-carboxylic acid.

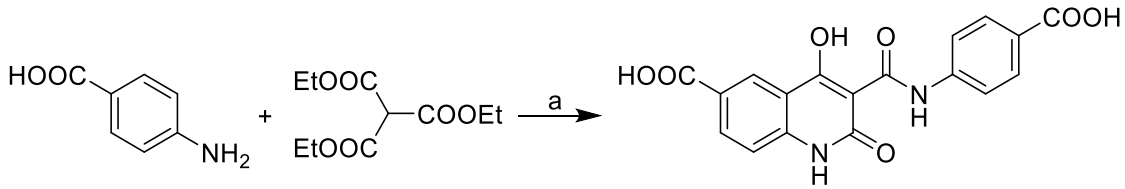

Scheme 1. Preparation of the target compound: (a) microwave irradiation

4-Aminobenzoic acid (0.7 g, 0.005 mol) was mixed with triethyl methanetricarboxylate (2.12 mL, 0.01 mol) and heated in microwave reactor at 50% of power during 15 min and 3 min at 90%. The temperature reached 231 °C during heating. Et_2O was added to the cooled mixture and the precipitate was washed with hot (55 °C) MeOH to obtain the pure product as a yellow crystalline compound. Yield 62%. Mp 340-350 °C. Anal. Calc. for $C_{18}H_{12}N_2O_7$ (368.29): C 58.70%, H 3.28%; found: C 58.09%, H 3.54%. HPLC purity 97.52%. UV (nm), λ_{max}/log ε: 251.3/3.53. IR (cm^{-1}): 3621, 1180 (OH), 3034 (CH_{arom}), 2970, 1689 (acid), 1680 (lactam), 1642 (C=O), 1635 (C = C_{cycle}), 1630 (amide), 1599 (Ph), 1520 (NH). ^{1}H NMR (DMSO-*d*$_6$, 500 MHz) δ: 7.41 (d, *J*=8.5 Hz, 1H), 7.70 (d, *J*=9.1 Hz, 2H), 7.90 (d, *J*=9.1 Hz, 2H), 8.15 (d, *J*=8.5 Hz, 1H), 8.50 (s, 1H), 12.40 (s, 1H), 12.95 (s, 1H), 16 (s, 1H). The FT-IR spectrum (Fig. 1) was recorded using KBr pellets on a DR/Jasco FT-IR 6300 spectrometer. The FT-Raman spectrum (Fig. 2) was obtained on a Bruker RFS 100/s, Germany. For excitation of the spectrum the emission of Nd: YAG laser was used, excitation wavelength 1064 nm, maximal power 150mW, measurement on solid sample.

3. Computational Details

Calculations of the wavenumbers, molecular geometry, polarizability values, frontier molecular orbital analysis were carried out with Gaussian 09 program [19] using the B3LYP/ 6-31G(d) quantum chemical calculation method. A scaling factor of 0.9613 is used to scale the theoretically obtained wavenumbers [20] and the assignments of the vibrational wavenumbers are done by using Gauss View [21] and GAR2PED software [22]. Parameters corresponding to optimized geometry of the title compound (Fig. 3) are given in Table 1. Jaguar 9.0 and

Schrodinger materials science suite 2015-4 was used for the investigation of the reactivity of the compound [23]. DFT calculations with the Jaguar were carried out using B3LYP exchange correlation functional, with 6-311++G(d,p), 6-31+G(d,p) and 6-311G(d,p) basis sets for the calculations of ALIE, Fukui functions and BDEs, respectively. Desmond program was used for MD simulations which was performed by OPLS 2005 force field [24], with simulation time set to 10 ns. The pressure was set at 1.0325 bar while temperature was set to 300 K. Cutoff radius was set to 12 Å, while the modelled system was of isothermal-isobaric (NPT) ensemble class. For the solvent of SPC model [25] was used here. For the modelling of system CPCHODQ6C molecule was placed alone into the cubic box with ~3000 water molecules. For the preparation of input files and output analysis Schrodinger materials science suite 2015-4 was used [26].

4. Results and Discussions

4.1 Optimized Geometrical Parameters

As far as we know, no X-ray crystallographic data of the title compound has yet been reported. However, the theoretical results (DFT) obtained are nearly comparable with the reported structural parameters of similar derivates. For the title compound the bond lengths of C_2-C_3 = 1.4084 Å, C_3-C_4 = 1.4130 Å and C_4-C_5 = 1.4045 Å and these values are greater than that of C_1-C_2 (1.3824 Å) and C_5-C_6 (1.3916 Å) due to adjacent quinoline ring and the reported values are C_2-C_3 = 1.4020 Å, C_3-C_4 = 1.4171 Å, C_5-C_4 = 1.4043 Å [27] and C2-C3=1.4121 Å, C3-C4=1.4079 Å and C5-C4=1.4045 Å respectively [28]. The values of bond lengths C_{12}-C_{14} (1.4579 Å) and C_{14}-C_{18} (1.4854 Å) are high which is due to the adjacent C=O and carbamoyl groups. Ranjith *et al* reported the corresponding values as C_{13}-C_{15}=1.4711 Å and C_{15}-C_{19}=1.4686 Å.[28]. The bond angle C_3-C_4-C_5 (119.5°) is lesser than 120° because of the presence of quinoline ring. The angles C_4-C_{13}-C_{14} and C_3-N_{10}-C_{12} are 121.2° and 126.0° respectively, which can be assumed as due to the presence of OH group which is electropositive. According to literature the corresponding reported bond angles are C_1-C_2-C_3 (119.6°), C_2-C_3-C_4 (119.4°), C_2-N_{14}-C_{20} (125.8°), C_3-C_{15}-C_{18} (121.3°) and N_{14}-C_{20}-C_{18} (114.2°) respectively [29]. The presence of higher electro negative group C=O would be the reason for the lesser bond angle of N_{10}-C_{12}-C_{14} (116.0°). The reported bond angle of N_{11}-C_{13}-C_{15} as 114.3° [28]

4.2 IR and Raman Spectra

The observed IR and Raman bands and calculated (scaled) wavenumbers and assignments are given in Table 2. The C_{12}=O_{16} and C_{13}=C_{14} stretching vibrations are assigned at 1678 cm^{-1} (DFT), 1670 cm^{-1} (IR) and at 1562 cm^{-1} (DFT), 1551 cm^{-1} (IR), 1548 cm^{-1} (Raman) respectively. The C=O stretching vibration in the spectra of carboxylic acid give rise to strong bands in the region 1600-1700 cm^{-1} [30]. The bands observed at 1746, 1741 cm^{-1}theoretically are assigned as C_{35}=O_{36}, C_{31}=C_{32} stretching modes of the title compound. The stretching band of C_{13}-O_{15} is expected in the region 1220 ± 40 cm^{-1} [31−33] and the band at 1292 cm^{-1} (DFT) is assigned as C-O stretching vibration of the title compound while the reported value is 1206 cm^{-1}(DFT) [31]. The O-H stretching vibration gives rise to a band at 3050 ± 150 cm^{-1} [30]. The band observed at 2666 cm^{-1} experimentally and 2793 cm^{-1} in DFT calculation is assigned as the O-H stretching vibration. The downshift of the OH stretching mode is due to the strong hydrogen bonded system present in the title compound as reported in literature [34]. The O-H in-plane and out-of-plane deformation modes are expected at 1395 ± 55 cm^{-1} and at 905 ± 70 cm^{-1} respectively [30]. For the title compound the band at 1352 cm^{-1} (DFT) is assigned as the in-plane O-H deformation band. Similarly, the band at 922 cm^{-1} (DFT) is assigned as the O-H out-of-plane deformation band of the title compound. Rajeev et al. [29] reported a band at 1412 cm^{-1} as the in-plane O-H deformation. The N-H stretching vibrations are expected [35] in the range 3500-3300 cm^{-1}. In the present study the bands observed at 3440, 3392 cm^{-1} in the IR spectrum and 3454 cm^{-1} theoretically are assigned as N-H stretching vibrational mode In the present case the N-H stretching mode splits into a doublet and downshifted from the computed value which indicates the weakening of the N-H bond [36,37]. N-H group shows bands at 1510-1500, 1350-1250 and 740-730 cm^{-1} [37]. According to literature if N-H is a part of a closed ring [38] the N-H deformation band is absent in the region 1510-1500 cm^{-1}. In the present case the N-H in-plane deformation band is observed at 1439 cm^{-1} theoretically.The out-of-plane deformation bands of N-H are expected in the range 650 ± 50 cm^{-1} and the bands observed at 612 cm^{-1} (DFT) are assigned as γN-H mode of the title compound. In the present case, the quinoline CC stretching ring modes are observed at 1413 cm^{-1} in the IR spectrum, 1414 cm^{-1} in the Raman spectrum, 1413 cm^{-1} theoretically with high Raman activity and the C-N stretching modes are at 1114 cm^{-1} in the IR spectrum, 1233, 1106,1082 cm^{-1} theoretically. Rajeev et al. reported the quinoline stretching modes at 1610, 1445, 1020 cm^{-1} (C-C), 1262 cm^{-1} (C-N) in the IR spectrum, 1609, 1051, 1022 cm^{-1} (C-C), 1202 cm^{-1} (C-N) in the Raman spectrum, 1607, 1433, 1045, 1035 cm^{-1} (C-C), 1270, 1230 cm^{-1} (C-N) theoretically [29]. The

DFT calculations give the C-H stretching modes of the phenyl ringI and phenyl ringII of the title compound at 3128, 3101, 3067 cm^{-1} and 3151, 3099, 3098, 3061 cm^{-1}. Similarly, the bands observed at 3132, 3103, 3078 cm^{-1} (Raman) and 3157, 2990 cm^{-1} (IR) are assigned as C-HI and C-HII stretching modes of the phenyl rings of parent molecule [30]. The bands observed at 1470, 1372 and 1593, 1505, 1314 cm^{-1}in IR spectrum, 1477 and 1602, 1503, 1382, 1323 cm^{-1} in Raman spectrum and at 1618, 1580, 1485, 1369, 1342 and 1609, 1591, 1538,1403,1321 cm^{-1} theoretically are assigned as phenyl rings stretching modes of the title compound which are expected in the region 1620-1250 cm^{-1} [30]. In asymmetric tri-substituted benzene, when all the three substituents are heavy, the ring breathing mode appears above 1100 cm^{-1} [31]. For the tri-substituted phenyl ring PhI, the ring breathing mode is assigned at 1066 cm^{-1} theoretically. Madhavan et al. [39] reported the ring breathing mode for a compound having two tri-substituted benzene rings at 1110 and 1083 cm^{-1} respectively. In the present case, the bands observed at 1070 cm^{-1} in Raman spectrum and 1072 cm^{-1} theoretically are assigned as the ring breathing mode of the phenyl ring II which is expected in region 1020-1070 cm^{-1} [32]. Panicker et al. [40] reported the ring breathing mode of di-substituted benzene at 1018 cm^{-1} (IR), 1034 cm^{-1} (Raman) and 1019 cm^{-1} (DFT). For the title compound, the bands observed at 1284 cm^{-1} (IR), 1134, 1099, cm^{-1} (Raman) and 1288, 1245, 1152, 1137, 1104 cm^{-1} (DFT) are assigned as the C-H in-plane bending modes of the phenyl rings. The C-H out-of-plane deformations are expected below 1000 cm^{-1}[31] and for the title compound the theoretical calculations give bands at 951, 949, 938, 925, 842, 828, 815, 794 cm^{-1} as γC-H modes of the phenyl rings. Experimentally these bands are observed at 970, 926, 841, 818, 799 cm^{-1} in the Raman spectrum.

4.3 Frontier Molecular Orbitals

Frontier molecular orbital study is used to explain the chemical behaviour and stability of the molecular system. The atomic orbital components of the frontier molecular orbitals are shown in (Fig. 4A, 4B, 4C, 4D). The delocalization of HOMO and LUMO over the molecular system shows the charge transfer within the molecular system. The HOMO-LUMO gap for CPCHODQ6C is found to be 2.646 eV. The chemical descriptors can be evaluated by using HOMO and LUMO orbital energies, E_{HOMO}, and E_{LUMO} as ionization energy $I= -E_{HOMO}$, electron affinity $A= -E_{LUMO}$, hardness $\eta = (I-A)/2$, chemical potential $\mu = -(I+A)/2$ and electrophilicity index $\omega = \mu^2/2\eta$ [41,42]. According to Kohn-Sham model, $I = -E_{HOMO} = 1.001$ [$-E_{HOMO}$(LBS)] -0.05 eV and $A= -E_{LUMO} = 1.0729$ [$-E_{LUMO}$(LBS)] -0.181 eV [43]. For the

title compound CPCHODQ6C, I = 8.54, A = 5.894, η = 1.323, μ = −7.217 and ω = 19.684 eV. The I, A, η, μ and ω values for halogen substituted CPCHODQ6C are tabulated in Table 3. For the title molecule (Fig. 4D) HOMO is delocalized over the phenyl group (PhII), amide group and partially over the quinoline ring while the LUMO is delocalized strongly over the entire molecule except carboxyl group of quinoline ring. For 7Cl (Fig. 4B) HOMO is delocalized strongly over the quinoline ring and substituted chlorine atom while LUMO is delocalized strongly over the entire molecule except NH groups. For 8Cl and 9Cl (Fig. 4B) HOMO is over the phenyl ring PhI and partially over the pyridine ring and LUMO is over the entire molecule except carboxyl group of PhI and carbonyl group of pyridine ring. For 7Br (Fig. 4C) HOMO is over the entire molecule except carboxyl group of PhI and LUMO is over the entire molecule. For 8Br and 9Br (Fig. 4C) HOMO is over the entire molecule except carboxyl group of PhI and carbonyl group of pyridine ring and LUMO is over the entire molecule except carboxyl group of PhI and NH group of pyridine ring. For 7F (Fig. 4A) HOMO is over the entire molecule except carboxyl group of PhI and NH of pyridine while LUMO is over the entire molecule except NH group of amide group. For 8F (Fig. 4A) HOMO is over the entire quinoline ring while for 9F (Fig. 4A) HOMO is over the entire molecule. LUMO is delocalized over the entire molecule except carboxyl group of PhI, carbonyl group of pyridine and NH group of amides for 8F and 9F. The chemical potential decreases for the halogen substitution in the order 7Cl, 8Cl, 9Cl < 7F, 8F, 9F < 7Br, 8Br, 9Br < CPCHODQ6C (Table 3) Chemical potential value of 8Cl is deviated maximum from the parent molecule while all other halogen substitution shows minimum deviation. Halogen substitution results in reduction in the μ value in comparison with the parent molecule and for 8Cl it is minimum. Halogen substitution also results a decrease in electrophilicity index and is minimum for 8Cl. Global hardness is higher for 8Cl because of its large HOMO-LUMO gap which results a decrease in polarizability.

4.4 Molecular Electrostatic Potential

Molecular electrostatic potential and electron density are related to each other to find the reactive sites for electrophilic and nucleophilic sites [44,45]. The negative (red and yellow) regions of MEP maps were related to electrophilic reactivity while the positive (blue) regions to nucleophilic reactivity. For the parent molecule (Fig. 5D) most electrophilic (red and Yellow) regions are C=O group of both carboxyl group, slightly over PhII and the nucleophilic regions (blue) are deeply over the NH bond of quinoline ring, slightly over the hydrogen atom

of the OH groups. For 7Cl, 8Cl and 9Cl (Fig. 5B) electrophilic regions are strongly over the carbonyl group of both carboxyl group and slightly over the phenyl ring while the nucleophilic regions are over the NH group of quinoline ring and slightly over the hydrogen atoms of the OH groups and more intense in the case of 8Cl. For fluorine substitution (Fig. 5A) the electrophilic regions are similar to that of chlorine substitution while the nucleophilic regions are same that of chlorine substitution but blue region of NH bond of quinoline in 8F is more pronounced. For bromine substitution (Fig. 5C) also the electrophilic and nucleophilic behaviour is identical to that of chlorine and fluorine substitution while blue region around bromine is higher than that in fluorine substitution. The nucleophilic region of fluorine substitution is less than that in chlorine and bromine substitution.

4.5 NBO Analysis

The natural bond orbitals (NBO) calculations were performed using NBO 3.1 program [46] and the important interactions are presented in Tables 4 and 5. The strong interactions are $LPO_{37}\rightarrow C_{35}-O_{36}$, $LPO_{36}\rightarrow C_{35}-O_{37}$ $LPO_{33}\rightarrow C_{31}-O_{32}$, $LPO_{32}\rightarrow C_{31}-O_{33}$, $LPN_{20}\rightarrow C_{18}-O_{19}$, $LPO_{15}\rightarrow C_{13}-C_{14}$, $LPN_{10}\rightarrow C_{12}-O_{16}$, $LPC_4\rightarrow C_{13}-C_{14}$ and $LPC_4\rightarrow C_5-C_6$ with energies, 21.44, 16.30, 21.43, 16.26, 28.99, 22.49, 27.67, 37.81 and 35.28 kcal/mol. 100% p−character is found in lone pairs of O_{37}, O_{36}, O_{33}, O_{32}, O_{16}, O_{15} and N_{10} atoms.

4.6 Nonlinear Optical Properties

The calculated first hyper polarizability of the title compound is 15.827×10^{-30} esu which is 121.75 times that of standard NLO material urea (0.13×10^{-30} esu) (Table 6) [47]. The reported value of first hyper polarizability of similar derivative is 2.24×10^{-30} esu [48]. The phenyl ring stretching vibrations at 1593, 1505 cm^{-1} in the IR spectrum have their counterparts in the Raman spectrum at 1602, 1503 cm^{-1} respectively with IR and Raman intensities are comparable. These types of organic molecules have conjugated π-electron system and large hyper polarizability which leads to nonlinear optical properties [49]. The C−N distances in the calculated molecular structure vary from 1.3745 to 1.4047 Å which are in between those of a CN single and double bond and this suggest an extended π-electron delocalization over the molecular system which is also responsible for the nonlinearity of the molecule [50]. We conclude that the title compound is an attractive object for future studies of non-linear optical properties.

4.7 ALIE surfaces and Fukui functions

Average local ionization energy (ALIE) is a quantum molecular descriptor which indicates the energy required to remove an electron from the molecule. So, we can say that the sites with least values of ALIE are more open for an electrophilic attack [51,52]. According to the equation given below ALIE is the sum of orbital energies weighted by the orbital density.

$$I(r)=\sum_i \frac{\rho_i(\vec{r})|\varepsilon_i|}{\rho(\vec{r})} \qquad (1)$$

Where $\rho_i(\vec{r})$ denotes electronic density of the i-th molecular orbital at the point $\vec{r}$, ε_i denotes orbital energy and $\rho(\vec{r})$ denotes total electronic density function. We have mapped the ALIE values with the electron density surface in order to understand the attacking sites of electrophiles. The ALIE figure is represented in Fig. 6. Here in this figure, we can see that benzene ring shows the least ALIE values that is 210.59 kcal/mol. On the other side in the close vicinity of hydrogen atoms H_{11}, H_{17}, H_{34}, H_{38}, H_{39} shows highest ALIE value 372.51 kcal/mol. The interesting molecular sites which are important in the view of local reactivity can be identified using Fukui functions. The functional derivative of chemical potential with respect to external potential is termed as Fukui functions. According to Maxwell's relations we can interpret this as the derivative of electronic density with respect to the number of electrons [53−55]. If we physically interpret the term, it is the change in electron density according to change in charge. These functions in Jaguar program are calculated with the help of finite difference approach, according to the following equations:

$$f^+ = \frac{\left(\rho^{N+\delta}(r)-\rho^N(r)\right)}{\delta} \qquad (2)$$

$$f^- = \frac{\left(\rho^{N-\delta}(r)-\rho^N(r)\right)}{\delta} \qquad (3)$$

where *N* stands for the number of electrons in reference state of the molecule, while δ stands for the fraction of electron which default value is set to be 0.01[55] . By plotting Fukui functions to electron density surfaces we get a lot of information about the important molecular sites acting as a reactive centre [51,52]. The Fukui function plot is represented in Fig. 7. The colour

coding in the plot is as follows, purple (positive) colour in Fukui function f^+ means the electron density has been increased by the addition of charges to the system while red (negative) colour in Fukui function f^- means the electron density has been diminished by the addition of charges. Electron density is increased in the near vicinity of carbon atom C_{21} and electron density is decreased near the O_{16}, O_{36}, O_{37} atoms.

4.8 Reactive and degradation properties based on autoxidation and hydrolysis

Degradation properties based on autoxidation and hydrolysis mechanisms are explained using RDFs and BDEs. Calculations of BDE for hydrogen abstraction allow the possibility to predict molecular sites where autoxidation process could start. It provides details about upto what extent some molecule are sensitive to presence of oxygen in open air, a parameter that is of very much importance in pharmaceutical industry. Forced degradation studies can also be studied using BDE, since they can be used for confirmation and determination of degradation path of some organic pharmaceutical molecule [56−58]. Wright et al. says that the target molecule is most vulnerable to autoxidation if the BDE for hydrogen abstraction ranges from 70 to 85 kcal/mol [59]. BDE values for hydrogen abstraction lower than 70 kcal/mol, are not suitable for the autoxidation mechanism since formed radicals are resistant for O_2 insertion [60−62]. Fig. 8 contains all BDE values for CPCHODQ6C. Red coloured values represent the BDE values for hydrogen abstraction and blue-coloured values correspond to the BDE values for the rest of the single acyclic bonds. All the BDE values of molecule are greater than 100 kcal/mol so we can say that the molecule is stable in the presence of oxygen. To find the extend of hydrolysis we have also calculated the RDF for the molecule. In Fig. 9 RDFs of atoms with the most pronounced interactions with water molecules are presented. In RDF plot, g(r) represents the probability of finding a particle in the distance r from another particle [63]. Results provided in Fig. 9 indicate that only ten atoms of CPCHODQ6C molecule have relatively significant interactions with water molecules. These atoms are C_{12}, C_{24}, O_{19}, O_{33}, O_{37} , H_{11}, H_{17}, H_{34}, H_{38}, H_{39} which shows similar g(r) profile. According to the maximal g(r) values the most important RDF is certainly for H_{34} atom. Here the presence of hydrogen atoms shows the low stability of the molecule in the surroundings of water, so the role of this title compound in the pharmaceutical industry is irrelevant.

4.9 Solubility parameter

One of the demanding fields in pharmaceutical is the development of new products and finding the active component. To be considered for the pharmaceutical drug production, the active ingredient has to fit in to certain physical properties such as stability, solubility etc. If the active component doesn't meet the required parameters, then these properties must be modified. One way to modify the properties without structural modification is to find a suitable excipient and mixing them up. Suitable excipient can be identified using experimental methods but its time consuming, while computational methods can be effectively used to narrow down the possibilities. Active component and excipient must be mutually compatible, one of the parameters for compatibility is the solubility parameter. Which means, the solubility parameter of the active component must have a value similar to the one of the excipient compounds [15−17]. Solubility parameter can be computationally predicted by applying the MD simulations and the following equation:

$$\delta = \sqrt{\frac{\Delta H_V - RT}{V_m}} \quad (1)$$

In this work, the solubility parameter has been calculated for the CPCHODQ6C molecule and it has been compared with three compounds frequently used as excipients polyvinylpyrrolidone polymer (PVP), maltose, and sorbitol). MD systems used to calculate this quantity consisted of 32 molecules placed in a cubic simulation box. Solubility parameters of all mentioned compounds have been summarized in Table 7. As indicated by the results presented in Table 7, the CPCHODQ6C molecule has the highest compatibility with the Maltose compound. In this case, the difference between corresponding values of solubility parameter is less than 0.2 $MPa^{1/2}$, indicating very high compatibility. Solubility parameter of sorbitol is higher than the solubility parameter of the CPCHODQ6C molecule, while PVP has lesser value than our title molecule. Therefore, the MD calculations suggest that it is reasonable to consider Maltose as an excipient for CPCHODQ6C molecule.

4.10 Molecular Docking

Antimalarial drugs constitute a major part of antiprotozoal drugs. Malaria remains a major health problem, mainly in sub-Saharan Africa and parts of Asia and South America [64] with over 200 million clinical infections and nearly half a million deaths annually. Malaria is caused

by protozoan parasites belonging to the genus Plasmodium and is transmitted via the bite of a female Anopheles mosquito. There are four major species of the parasite that cause malaria in humans, namely, Plasmodium falciparum, P. vivax, P. ovale and P. malaria, while a fifth parasite, P. knowlesi, is now recognized [65]. Historically, a range of drugs has been used to treat or prevent malaria, including several derived from the quinoline ring system such as quinine, chloroquine (CQ), amodiaquine, piperaquine, mefloquine, and primaquine [66]. Quinoline and its related derivative comprise a class of heterocycles, which has been exploited immensely than any other nucleus for the development of potent antimalarial agents. Various chemical modifications of quinoline have been attempted to achieve analogs with potent antimalarial properties against sensitive as well as resistant strains of Plasmodium sp., together with minimal potential undesirable side effects [67]. From PASS (Prediction of Activity Spectra) [68] analysis we have to choose the favorable target for docking study and different types of activities predicted as in Table 8. We choose the activity ubiquinol-cytochrome-c reductase inhibitor with Pa value 0.858 and high-resolution crystal structure of corresponding receptor atovaquone-inhibited cytochrome BC1 complex with (PDB ID: 4PD4) was downloaded from the RCSB protein data bank website. Atovaquone is a drug that inhibits the respiratory chain of Plasmodium falciparum, but with serious limitations like known resistance, low bioavailability and high plasma protein binding [69]. cyt bc1 inhibitors are generally classified as slow-onset anti-malarials, we found that a single dose of endochin-like quinolone-400 (ELQ-400) rapidly induced stasis in blood-stage parasites, which was associated with a rapid reduction in parasitemia in vivo. ELQ-400 also exhibited a low propensity for drug resistance and was active against atovaquone-resistant P. falciparum strains with point mutations in cyt bc1. ELQ-400 shows that cyt bc1 inhibitors can function as single-dose, blood-stage anti-malarials and is the first compound to provide combined treatment, prophylaxis, and transmission blocking activity for malaria after a single oral administration [70]. This remarkable efficacy suggests that metabolic therapies, including cyt bc1 inhibitors, may be valuable additions to the collection of single-dose anti-malarials in current development. All docking calculations were performed on AutoDock4.2 [71], Auto Dock-Vina software [72] and as in literature [73]. The amino acids of the receptor Tyr275, Asn96, Asn271 forms H-bond with OH group and other electrostatic interactions are detailed in Fig. 10. The docked ligand forms a stable complex with the receptors atovaquone−inhibited cytochrome BC1 complex as depicted in Fig. 11 and the binding free energy value is -9.1 kcal/mol (Table 9). The docked ligand is embedded with the catalytic site of cytochrome BC1 complex as shown in Fig. 12. These preliminary results suggest that the compound having inhibitory activity against the

antimalarial receptor atovaquone−inhibited cytochrome BC1 complex. Thus, the title compound can be developed as drug used for the treatment of malaria.

4.11 Drug-Likeness Study

The drug-likeness characteristics of the CPCHODQ6C molecule were predicted using validated free web tool SwissADME [74] .The results were tabulated as in Table 10. According to Lipinski *et al* [75] the title compound must have 5 special features as follows 1- MlogP ≤ 5, 2- molecular weight (MW) ≤ 500 gm/mol, 3-number of H-bond accepter (HBA) ≤ 10 and number of H-Bond donors (HBD) ≤ 5, 4- number of rotable bonds (nRot) ≤ 10 and 5- topological Polar Surface Area (TPSA) < 140$Å^{2.}$ From the Table 10 our synthesized compound shows good agreement with the criteria stated by Lipinski rules. Bioavailability radar of the CPCHODQ6C was created using SwissADME (Fig. 13) and shows that the compound has a moderate water solubility and low gastrointestinal absorption. Hence it may not be suitable for oral administration.

5 Conclusions

The vibrational spectroscopic studies of 3-[(4-carboxyphenyl) carbamoyl]-4-hydroxy-2-oxo-1, 2-dihydroquinoline-6-carboxylic acid in the ground state were reported theoretically and experimentally. Potential energy distribution of normal mode vibration was done using GAR2PED programme. The vibrational wave number of the title compound successfully analysed. For the title compound HOMO is delocalized over the phenyl group, amide group and LUMO is over the entire molecule except carboxyl group of quinoline ring. In addition to that the halogen substituted HOMO-LUMO calculation showed a decrease in the electrophilicity index and is minimum for substituted chlorine at the eighth position of the compound. The molecular electrostatic potential analysis results that the negative charge covers part of the oxygen atom in carboxylic acid and positive charge over the nitrogen atom in the quinoline ring. NBO analysis predicts a strong interactions $LPO_{37}\rightarrow C_{35}-O_{36}$, $LPO_{36}\rightarrow C_{35}-O_{37}$ $LPO_{33}\rightarrow C_{31}-O_{32}$, $LPO_{32}\rightarrow C_{31}-O_{33}$, $LPN_{20}\rightarrow C_{18}-O_{19}$, $LPO_{15}\rightarrow C_{13}-C_{14}$, $LPN_{10}\rightarrow C_{12}-O_{16}$, $LPC_{4}\rightarrow C_{13}-C_{14}$ and $LPC_{4}\rightarrow C_{5}-C_{6}$. The calculated first hyperpolarizability of the material is 121.75 times greater than the standard NLO material, so we can say that the compound is optically active. By DFT calculations we were able to calculate the ALIE values,

beside benzene ring, we have determined H_{11}, H_{17}, H_{34}, H_{38}, H_{39} are prone to electrophilic attacks. Thanks to the mapping of the Fukui function values to the electron density surface we have also determined that carbon atom C_{21} and O_{16}, O_{36}, O_{37} are important reactive centres. Calculation of BDE showed that title molecule is not sensitive in the water surroundings towards auto oxidation mechanisms. The presence of hydrogen atoms in the RDF shows the low stability of the title compound in the degradation processes. The MD calculations of solubility parameter suggests that it is reasonable to consider Maltose as an excipient for CPCHODQ6C molecule. By molecular docking the compound forms a stable complex with ubiquinol-cytochrome–c reductase inhibitor as is evident from the binding affinity values.

Acknowledgments

Part of this work has been performed with the support from Schrödinger Inc. Authors would like to extend their appreciation to the department of physics, University of Novi Sad for the Molecular dynamics simulations.

References

[1] Y. Bouzian, K. Karrouchi, Y. Sert, C.H. Lai, L. Hani, N.H. Ahabchane, A. Talbaoui, J. T. Mague, E.M. Essassi, Synthesis, spectroscopic characterization, crystal structure, DFT, molecular docking and in vitro antibacterial potential of novel quinoline derivatives J. Mol. Struct. 1209 (2020) 127940.

[2] S. Tewari, P.M.S. Chauhan, A.P. Bhaduri, M. Fatima, R.K. Chatterjee, Synthesis and Anti filarial agents Bioorg. Med. Chem. Lett. 10 (2000) 1409−1412.

[3] Y. Bouziana, Y. Sert, K. Khalid, L.V. Meervelt, K. Chkiratea, Lhassan Mahi, N.H. Ahabchane, A. Talbaoui, E.M. Essassi, Synthesis, spectroscopic characterization, DFT, molecular docking and in vitro antibacterial potential of novel quinoline derivatives, J. Mol. Struct.1246 (2021) 131217.

[4] B. Sureshkumar, Y.S. Mary, C.Y. Panicker, S. Suma, Stevan Armaković, Sanja J. Armaković, C.Van Alsenoy, B. Narayana Quinoline derivatives as possible lead compounds for anti-malarial drugs: spectroscopic, DFT and MD study, Arab. J. Chem.13 (2020) 632-648.

[5] R.F. Hector, An overview of anti-fungal drugs and their use for treatments of deep and superficial mycoses in animals, Clin. Tech. Small Anim. Pract. 20 (2005) 240−249.

[6] A. Nayyar, A. Malde, E. Coutinho, R. Jain, Synthesis, anti-tuberculosis activity and 3D-QSAR study of ring-substituted-2/4-quinoline carbaldehyde derivatives, Bioorg. Med. Chem. 14 (2006) 7302−7310.

[7] B. Sureshkumar, Y.S Mary, C.Y. Panicker, K.S. Resmi, S. Suma, S. Armaković, S.J. Armaković, C. Van Alsenoy. Spectroscopic analysis of 8-hydroxyquinoline-5-sulphonic acid and investigation of its reactive properties by DFT and molecular dynamics simulations. J. Mol. Struct. 1150 (2017) 540−552.

[8] G. Bandoli, A. Dolmella, F. Tisato, M. Porchia, F. Refosco Mononuclear six coordinated Ga (III) complexes, a comprehensive survey Coord. Chem. Rev. 253 (2009) 56−77.

[9] M.J. Hannon, Metal based anticancer drugs, from a past anchored in platinum chemistry to a post genomic future of diverse chemistry and biology. Pure Appl. Chem. 79 (2007) 2243−2261.

[10] R.T. Ulahannan, C.Y. Panicker, H.T. Varghese, R. Musiol, J. Jampilek, C. Van Alsenoy, J.A. War, S.K. Srivastava, Molecular structure, FT-IR, FT-Raman, NBO, HOMO and LUMO, MEP, NLO and molecular docking study of 2-[(E)-2-(2-bromophenyl)-ethenyl quinoline-6-carboxylic acid Spectrochim. Acta. 151 (2015) 184−197.

[11] S.A. Khan, A.M. Asiri, S.H. Al-Thaqafy, H.M.F. Aidallah, S.A. El-Daly, Synthesis, characterization and spectroscopic behavior of novel 2-oxo-1,4-disubstituted-1,2,5,6-tetrahydrobenzo[h]quinoline-3-carbonitrildyes, Spectrochim. Acta 133 (2014) 141−148.

[12] C.B. Sangani, J.A. Makawana, X. Zhang, S.C. Teraiya, I. Lin, H.L. Zhu, Design, synthesis and molecular modeling of pyrazole-quinoline-pyridine hybrids as a new class of antimicrobial and anticancer agents, Eur. J. Med. Chem.76 (2014) 549−557.

[13] V. Arjunana, S. Mohanb, P.S. Balamourougan, P. Ravindran, Quantum chemical and spectroscopic investigations of 5-aminoquinoline, Spectrochim. Acta Part A 74 (2009) 1215–1223.

[14] S. Armakovic, S.J. Armakovic, J.P. Setrajcic, I.J. Serajcic, Active components of frequently used β- blockers from the aspect of computational study. J. Mol. Model, 18 (2012) 4491−4501.

[15] D.J. Greenhalgh, A.C. Williams, P. Timmins, P. York, Solubility parameters as predictors of miscibility in solid dispersions, J. Pharm. Sci. 88 (1999) 11821−190.

[16] R.C. Rowe, Adhesion of film coatings to tablet surfaces a theoretical approach based on solubility parameters, Int. J. Pharm. 41(1988) 219−222.

[17] R.C. Rowe, Interactions in coloured powders and tablet formulations: a theoretical approach based on solubility parameters, Int. J. Pharm. 53 (1989) 47−51.

[18] J. Jampilek, R. Musiol, M. Pesko, K. Kralova, M. Vejsova, J. Carroll, A. Coffey, J. Finster, D. Tabak, H. Niedbala, V. Kozik, J. Polanski, J. Dohnal, Ring-substituted 4-hydroxy-1H-quinolin-2-ones: Preparation and biological activity. Molecules, 14 (2009) 1145−1159.

[19] Gaussian 09, Revision B.01, M.J. Frisch, G.W. Trucks, H.B. Schlegel, G.E. Scuseria, M.A. Robb, J. R. Cheeseman, G. Scalmani, V. Barone, B. Mennucci, G.A. Petersson, H. Nakatsuji, M. Caricato, X. Li, H. P. Hratchian, A.F. Izmaylov, J. Bloino, G. Zheng, J.L. Sonnenberg, M. Hada, M. Ehara, K. Toyota, R. Fukuda, J. Hasegawa, M. Ishida, T. Nakajima, Y. Honda, O. Kitao, H. Nakai, T. Vreven, J.A. Montgomery, Jr., J. E. Peralta, F.Ogliaro, M. Bearpark, J.J. Heyd, E. Brothers, K.N. Kudin, V.N. Staroverov, T. Keith, R. Kobayashi, J. Normand, K. Raghavachari, A. Rendell, J.C. Burant, S.S. Iyengar, J. Tomasi, M. Cossi, N. Rega, J M. Millam, M. Klene, J.E. Knox, J.B. Cross, V. Bakken, C. Adamo, J. Jaramillo, R. Gomperts, R.E. Stratmann, O. Yazyev, A.J. Austin, R. Cammi, C. Pomelli, J.W. Ochterski, R.L. Martin, K. Morokuma, V.G. Zakrzewski, G.A. Voth, P. Salvador, J.J. Dannenberg, S. Dapprich, A.D. Daniels, O. Farkas, J.B. Foresman, J.V. Ortiz, J. Cioslowski, and D.J. Fox, Gaussian, Inc., Wallingford CT, 2010.

[20] J.B. Foresman, in: E. Frisch (Ed.), Exploring Chemistry with Electronic Structure Methods: A Guide to Using Gaussian, Gaussian Inc., Pittsburg, PA, 1996.

[21] Gauss View, Version 5, R. Dennington, T. Keith, J. Millam, SemichemInc., Shawnee Mission, KS, 2009.

[22] J.M.L. Martin, C. Van Alsenoy, GAR2PED, A Program to Obtain a Potential Energy Distribution from a Gaussian Archive Record, University of Antwerp, Belgium, 2007.

[23] A.D. Becke, Density-functional thermochemistry. III. The role of exact exchange, J. Chem. Phys. 98 (1993) 5648−5652.

[24] J.L. Banks, H.S. Beard, Y. Cao, A.E. Cho, W. Damm, R. Farid, A.K. Felts, T.A. Halgren, D.T. Mainz, J.R. Maple, Integrated modelling program, applied chemical theory (IMPACT), J. Comput. Chem. 26 (2005) 1752–1780.

[25] H.J. Berendsen, J.P. Postma, W.F. van Gunsteren, J. Hermans, Interaction models for water in relation to protein hydration, in Intermolecular forces. 1981, Springer. p. 331−342.

[26] Schrödinger Release 2015-4: Maestro, version 10.4, Schrödinger, LLC, New York, NY, 2015.

[27] J. Chowdhury, M.Ghosh, T.N. Misra, Surface enhanced Raman scattering of 2,2-biquinoline adsorbed on colloidal silver particles, Spectrochim. Acta 56 (2000) 2107−2115.

[28] P.K. Ranjith, Y. Sheena Mary, C. Yohannan Panicker, P.L. Anto, Stevan Armakovic, Sanja J. Armakovic, Robert Musiol, Josef Jampilek, C. Van Alsenoy, New quinolone derivative: Spectroscopic characterization andreactivity study by DFT and MD approaches, J. Mol. Struct. 1135 (2017) 1−14.

[29] R.T. Ulahannan, C.Y. Panicker, H.T. Varghese, C. Van Alsenoy, R. Musiol, J. Jampilek, P.L. Anto Spectroscopic (FT-IR, FT-Raman) investigations and quantum chemical calculations of 4-hydroxy-2-oxo-1,2-dihydroquinoline-7-carboxylic acid Spectrochim. Acta 121 (2014) 404−414.

[30] N.P.G. Roeges, A Guide to the Complete Interpretation of the Infrared spectra of Organic Compounds, Wiley, New York 1994.

[31] G. Varsanyi, Assignments of Vibrational Spectra of Seven Hundred Benzene Derivatives, Wiley, New York 1974.

[32] N.B. Colthup, L.H. Daly, S.E. Wiberly, Introduction to IR and Raman Spectroscopy, Academic Press, New York, 1990.

[33] R.M. Silverstein, F.X. Webster, Spectrometric Identification of Organic Compounds, ED. 6, John Wiley, Asia, 2003.

[34] Y.S. Mary, P.J. Jojo, C. Van Alsenoy, M. Kaur, M.S. Siddegowda, H.S. Yathirajan, H.I.S. Nogueira, S.M.A. Cruz, Vibrational spectroscopic studies (FT-IR, FT-Raman, SERS) and quantum chemical calculations on cyclobenzaprinium salicylate, Spectrochim. Acta 120 (2014) 340−350.

[35] L.J. Bellamy, The IR spectra of Complex Molecules, John Wiley and Sons, New York 1975.

[36] S.H.R. Sebastian, M.A. Al-Alshaikh, A.A. El-Emam, C.Y. Panicker, J. Zitko, M. Dolezal, C. Van Alsenoy, Spectroscopic quantum chemical studies, Fukui functions, in vitro antiviral activity and molecular docking of 5-chloro-N-(3-nitrophenyl) pyrazine-2-carboxamide, J. Mol. Struct. 1119 (2016) 188−199.

[37] V.V. Menon, E. Foto, Y.S. Mary, E. Karatas, C.Y. Panicker, G. Yalcin, S. Armakovic, S.J. Armakovic, C. Van Alsenoy, I. Yildiz, Vibrational spectroscopic analysis, molecular dynamics simulations and molecular docking study of 5-nitro-2-phenoxymethyl benzimidazole, J. Mol. Struct. 1129 (2017) 86−97.

[38] G. Socrates, Infrared Characteristic Group Frequencies, John Wiley and Sons, NewYork, 1981.

[39] V.S. Madhavan, H.T. Varghese, S. Mathew, J. Vinsova, C.Y. Panicker, FT-IR, FT-Raman and DFT calculations of 4-Chloro-2-(3,4-dichlorophenyl carbamoyl) phenyl acetate, Spectrochim. Acta. 72 (2009) 547−553.

[40] C.Y. Panicker, K.R. Ambujakshan, H.T. Varghese, S. Mathew, S. Ganguli, A.K. Nanda, C. Van Alsenoy, FT-IR, FT-Raman and DFT calculations of 3-{[(4-fluorophenyl)methylene]amino}-2-phenylquinazolin-4(3H)-one, J. Raman. Spectrosc. 40 (2009) 527−536.

[41] A.S. El-Azab, Y.S. Mary, C.Y. Panicker, A.A.-M A-Aziz, A. Magda, El-Sherbeny, C. Van Alsenoy, DFT and experimental (FT-IR and FT-Raman) investigation of vibrational spectroscopy and molecular docking studies of 2-(4-oxo-3-phenyl-3,4-dihydroquinazolin-2-ylthio)-N-(3,4,5 trimethoxy phenyl) acetamide, J. Mol Struct. 1113 (2016) 133−145.

[42] M. Miar, A. Shiroudi, K. Pourshamsian, A.R. Oliaey, F. Hatamjafar, Theoretical investigations on the HOMO–LUMO gap and global reactivity descriptor studies, natural bond orbital, and nucleus-independent chemical shifts analyses of 3-phenylbenzo thiazole-2(3H)-imine and its para-substituted derivatives: Solvent and substituent effects, J. Chem. Res. January-February (2021) 147–158.

[43] C.G. Zhan, J.A. Nichols, D.A. Dixon, Ionization Potential, Electron Affinity, Electronegativity, Hardness, and Electron Excitation Energy: Molecular Properties from Density Functional Theory Orbital Energies, J. Phys. Chem. A 107 (2003) 4184-4195.

[44] F.J. Luque, J.M. Lopez, M. Orozco, Perspective on electrostatic interactions of a solute with a continuum, a direct utilization of ab initio molecular potentials for the prevision of solvent effects, Theor. Chem. Acc. 103 (2000) 343−345.

[45] P. Politzer, J.S. Murray, in: D.L. Beveridge, R. Lavery, (Eds.), Theoretical Biochemistry and Molecular Biophysics, Springer, Berlin, 1991.

[46] NBO Version 3.1, E.D. Glendening, A.E. Reed, J.E. Carpenter, F. Weinhold.

627 [47] C. Adant, M. Dupuis, J.L. Bredas, Ab initio study of the nonlinear optical properties of
628 urea, electron correlation and dispersion effects, Int. J. Quantum. Chem. 56 (1995)
629 497−507.
630 [48] G. Purohit, G.C. Joshi, Second order polarizabilities of some quinolines, Indian J. Pure
631 Appl. Phys. 41 (2003) 922−927.
632 [49] Y.S. Mary, C.Y. Panicker, H.T. Varghese, K. Raju, T.E. Bolelli, I. Yildiz, C.M.
633 Granadeiro, H.I.S. Nogueira, Vibrational spectroscopic studies and computational
634 study of 4-fluoro-N-(2'-hydroxy-4'-nitrophenyl) phenylacetamide, J. Mol. Struct. 994
635 (2011) 223−231.
636 [50] S.R. Sheeja, N.A. Mangalam, M.R.P. Kurup, Y.S. Mary, K. Raju, H.T. Varghese, C.Y.
637 Panicker, Vibrational spectroscopic studies and computational study of quinoline-
638 2carbaldehyde benzyol hydrazone, J. Mol. Struct. 973 (2010) 36−46.
639 [51] J.S. Murray, J.M. Seminario, P. Politzer, P. Sjoberg, Average local ionization energies
640 computed on the surfaces of some strained molecules, Int. J. Quantum Chem. 38(S24)
641 (1990) 645−653.
642 [52] P. Politzer, F. Abu-Awwad, J.S. Murray, Comparison of density functional and
643 Hartree–Fock average local ionization energies on molecular surfaces, Int. J.
644 Quantum Chem. 69(4) (1998) 607−613.
645 [53] A. Toro-Labb, P. Jaque, J.S. Murray, P. Politzer, Connection between the average
646 local ionization energy and the Fukui function, Chem. Phys. Lett. 407 (2005)
647 143−146.
648 [54] R.G. Parr, Density Functional Theory of Atoms and Molecules, in Horizons of
649 Quantum Chemistry, Springer (1980) 5−15.
650 [55] A. Michalak, F. De Proft, P. Geerlings, R. Nalewajski, Fukui functions from the
651 relaxed Kohn-Sham orbitals, J. Phys. Chem. A 103 (1999) 762−771.
652 [56] X. Ren, Y. Sun, X. Fu, L. Zhu, Z. Cui, DFT comparison of the OH-initiated
653 degradation mechanisms for five chlorophenoxy herbicides, J. Mol. Model. 19 (2013)
654 2249−2263.
655 [57] l. Ai, J.Y. Liu, Mechanism of OH-initiated atmospheric oxidation of E/Z-CF3CF=
656 CFCF3: a quantum mechanical study, J. Mol. Model. 20 (2014) 1−10.
657 [58] W. Sang-aroon, V. Amornkitbamrung, V. Ruangpornvisuti, A density functional
658 theory study on peptide bond cleavage at aspartic residues: direct vs cyclic
659 intermediate hydrolysis, J. Mol. Model. 19 (2013) 5501−5513.

[59] J. Kieffer, É. Brémond, P. Lienard, G. Boccardi, In silico assessment of drug substances chemical stability, J. Mol. Struct. THEOCHEM. 954 (2010) 75−79.

[60] J.S. Wright, H. Shadnia, L.L. Chepelev, Stability of carbon-centered radicals: Effect of functional groups on the energetics of addition of molecular oxygen, J. Comput. Chem. 30 (2009) 1016−1026.

[61] P. Lienard, J. Gavartin, G. Boccardi, M. Meunier, Predicting drug substances autoxidation, Pharm. Res. 32 (2015) 300−310.

[62] T. Andersson, A. Broo, E. Evertsson, Prediction of Drug Candidates' Sensitivity Toward Autoxidation: Computational Estimation of C-H Dissociation Energies of Carbon-centered Radicals, J. Pharm. Sci. 103 (7) (2014) 1949−1955.

[63] R.V. Vaz, J.R. Gomes, C.M. Silva, Molecular dynamics simulation of diffusion coefficients and structural properties of ketones in supercritical CO_2 at infinite dilution, J. Supercritic. Fluids, 107 (2016) 630−638.

[64] M. Cunha-Rodrigues, M. Prudencio, M.M. Mota, W. Haas, Antimalarial drugs–host targets (re)visited, Biotechnol. J. 1 (2006) 321−332.

[65] C. Daneshvar, T.M. Davis, J. Cox-Singh, M.Z. Rafa'ee, S.K. Zakaria, P.C. Divis, B. Singh, Clinical and laboratory features of human Plasmodium knowlesi infection, Clin. Infect. Dis. 49 (2009) 852−860.

[66] B. Gunsaru, S.J. Burgess, W. Morrill, J.X. Kelly, S. Shomloo, M.J. Smilkstein, K. Liebman, D.H. Peyton, Siplified reversed chloroquines to overcome malaria resistance to quinoline-based drugs, Antimicrob. Agents Chemother. 61 (2017) 1913−1916.

[67] B. Sandhya, S. Kumar, S. Drabu, R. Kumar, Structural modifications of quinoline-based antimalarial agents: Recent developments, J. Pharm. Bioallied. Sci. 2 (2010) 64−71.

[68] A. Lagunin, A. Stepanchikova, D. Filimonov, V. Poroikov, PASS: prediction of activity spectra for biologically active substances, Bioinformatics 16 (2000) 747−748.

[69] A.C.R. Sodero, B. Abrahim-Vieira, P.H.M. Torres, P.G. Pascutti, C.R.S. Garcia, V.F. Ferreira, D.R. da Rocha, S.B. Ferreira, F.P. Silva, Atovaquone is a drug that inhibits the respiratory chain of Plasmodium falciparum, but with serious limitations like known resistance, low bioavailability and high plasma protein binding, Mem. Inst. Oswaldo. Cruz, 112 (2017) 299−308.

[70] A.M. Stickles, L.M. Ting, J.M. Morrisey, Y. Li, M.W. Mather, E. Meermeier, A.M. Pershing, I.P. Forquer, G.P. Miley, S. Pou, R.W. Winter, D.J. Hinrichs, J.X. Kelly, K. Kim, A.B. Vaidya, M.K. Riscoe, A. Nilsen, Inhibition of Cytochrome bc1 as a Strategy for Single-Dose, Multi-Stage Antimalarial Therapy, Am. J. Trop. Med. Hyg. 92 (2015) 1195−1201.

[71] G.M. Morris, R. Huey, W. Lindstrom, M.F. Sanner, R.K. Belew, D.S. Goodsell, A.J. Olson, Autodock4 and AutoDockTools4: automated docking with selective receptor flexibility, J. Comput. Chem. 16 (2009) 2785−2791.

[72] O. Trott, A.J. Olson, AutoDock Vina: Improving the speed and accuracy of docking with a new scoring function, efficient optimization and multithreading, J. Comput. Chem. 31 (2010) 455−461.

[73] J.A. War, K. Jalaja, Y.S. Mary, C.Y. Panicker, S. Armakovic, S.J. Armakovic, S.K. Srivastava, C. Van Alsenoy, Spectroscopic characterization of 1-[3-(1H-imidazol-1-yl)propyl]-3-phenylthiourea and assessment of reactive and optoelectronic properties employing DFT calculations and molecular dynamics simulations, J. Mol. Struct. 1129 (2017) 72−85.

[74] I. Çapan, S. Servi, I. Yıldırım, Y. Sert, Synthesis, DFT Study, Molecular Docking and Drug Likeness Analysis of the New Hydrazine-1-Carbothioamide,Triazole and Thiadiazole Derivatives: Potential Inhibitors of HSP90, ChemistrySelect 6 (2021) 5838−5846.

[75] C.A. Lipinski, F. Lombardo, B.W. Dominy P.J. Feeney, Experimental and computational approaches to estimate solubility and permeability in drug discovery and development settings, Adv Drug Deliv. Rev. 23 (1997) 3−25.

Figure Caption

Fig 1 FT-IR

Fig 2 FT-Raman

Fig 3 Molecule

Fig 4A HOMO-LUMO -1

Fig 4B HOMO-LUMO-2

Table Caption

Highlights

* The quinoline derivative was synthesized and FT-IR and FT-Raman spectra were measured
* DFT calculations were performed
* Most reactive sites were identified
* Results of halogen substitution in the calculations of chemical descriptors and HOMO-LUMO gap were calculated.
* Molecular docking studies between the title compound and 4PD4 protein were performed.

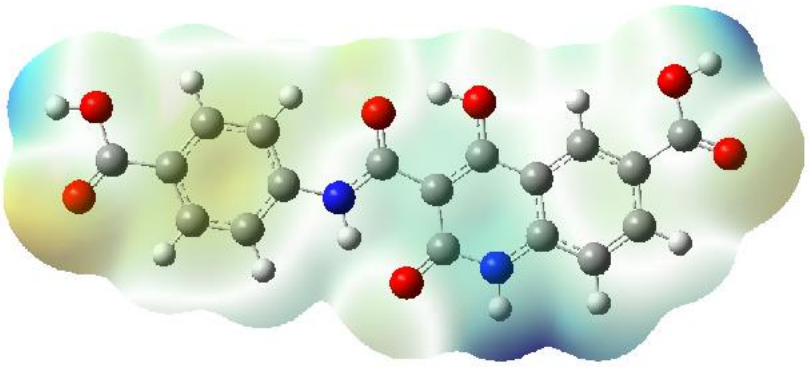

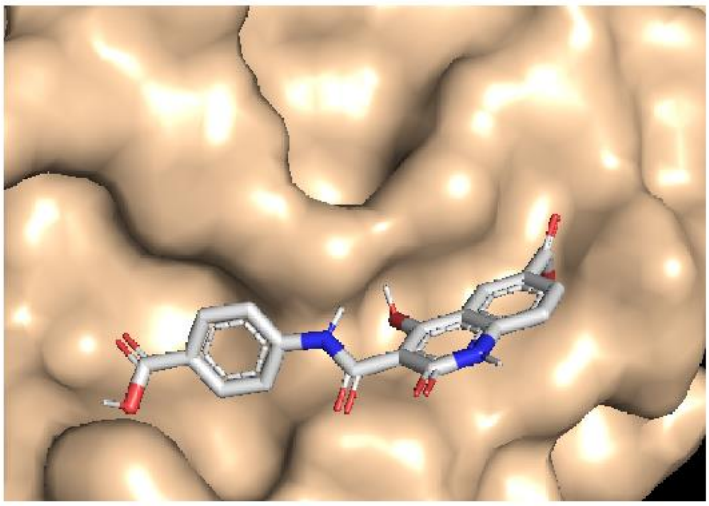

Scheme 1. Preparation of the target compound: (a) microwave irradiation

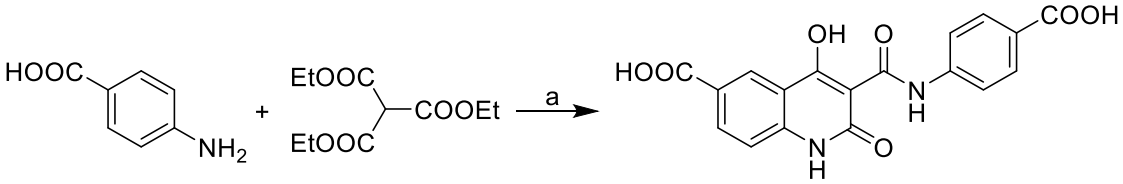

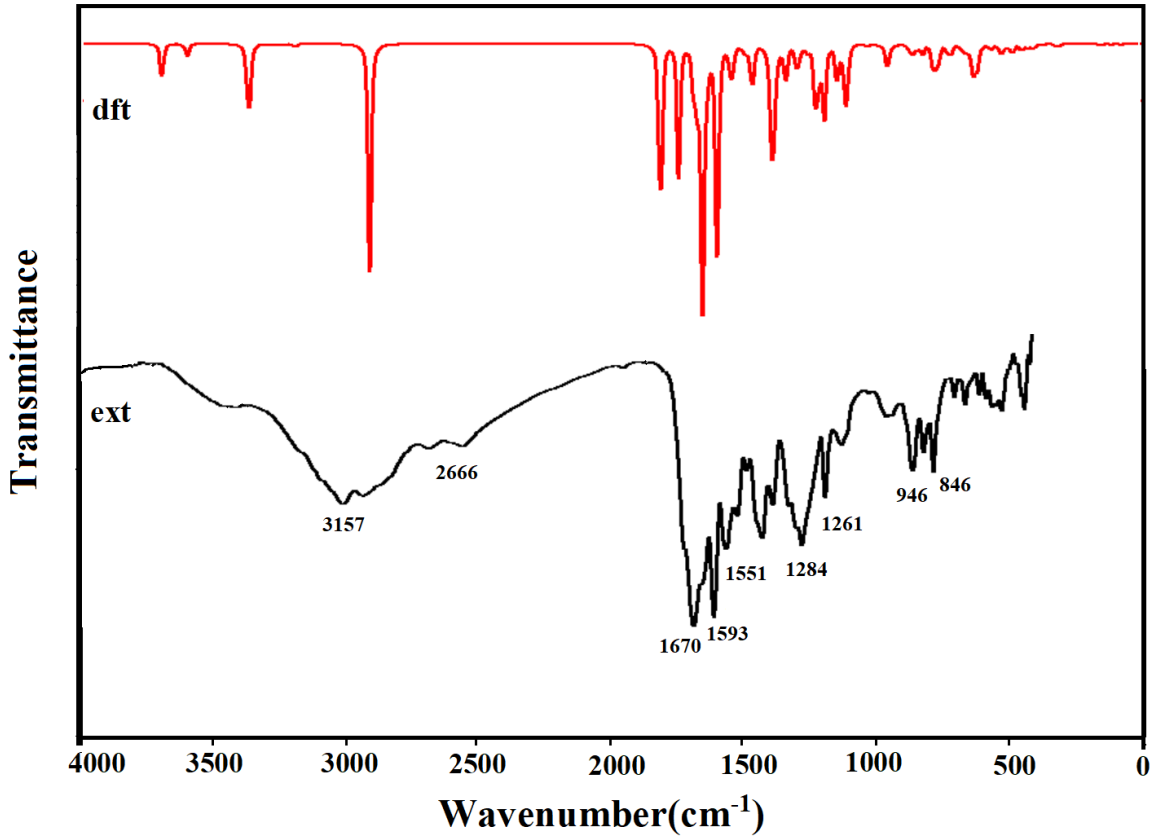

Fig. 1. FT-IR spectrum of CPCHODQ6C

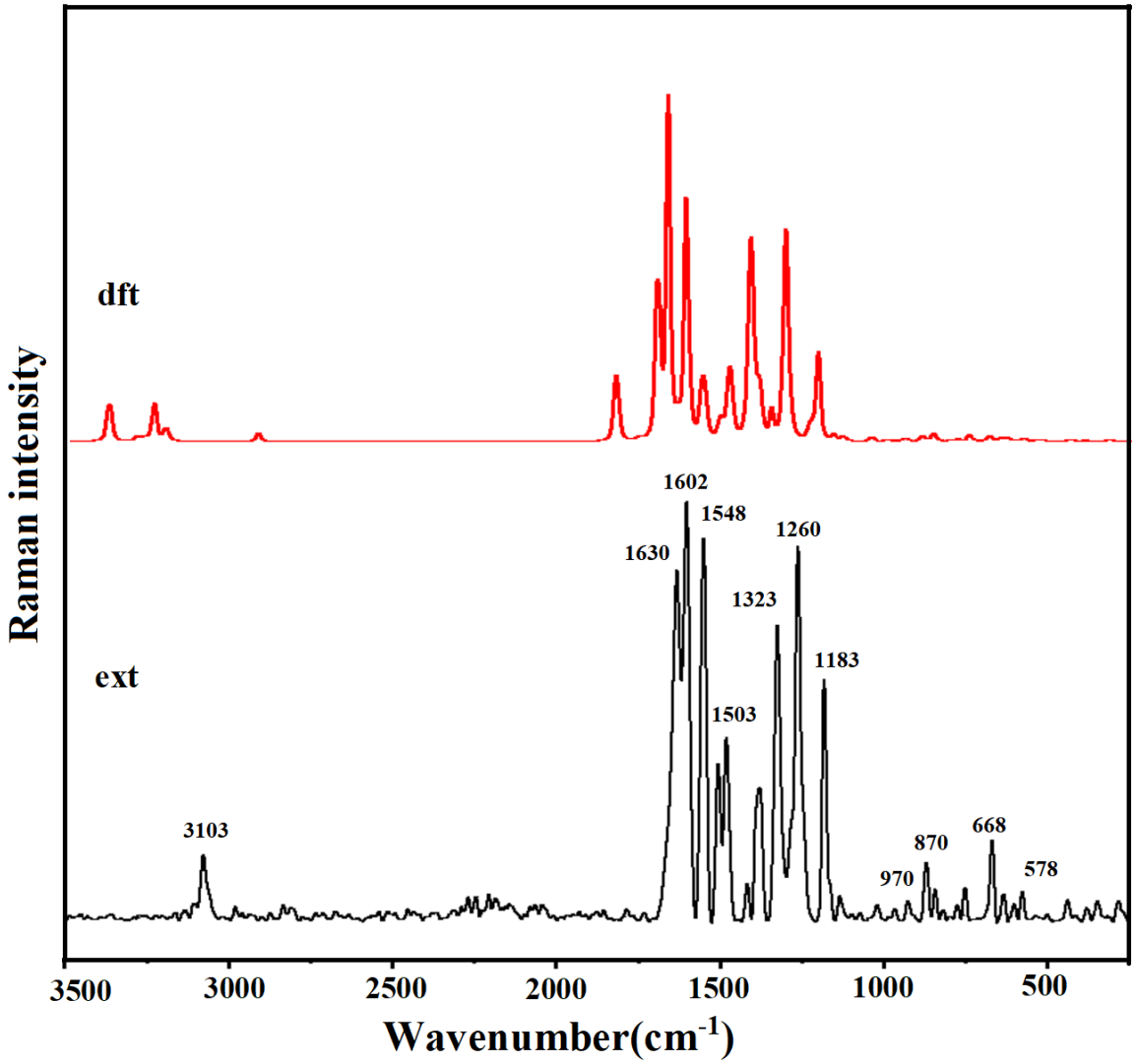

Fig. 2. FT-Raman spectrum of CPCHODQ6C

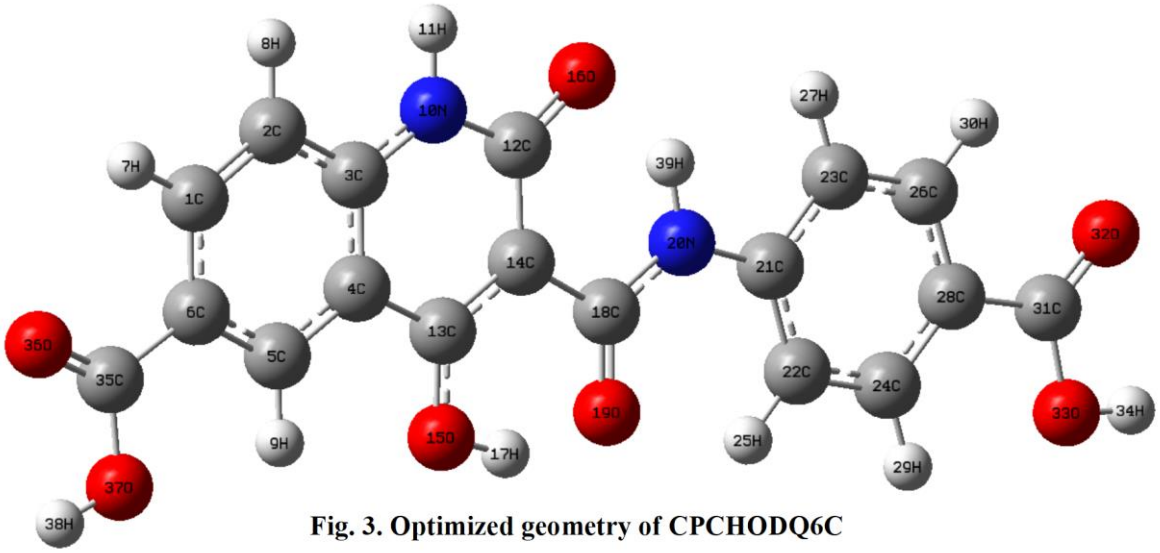

Fig. 3. Optimized geometry of CPCHODQ6C

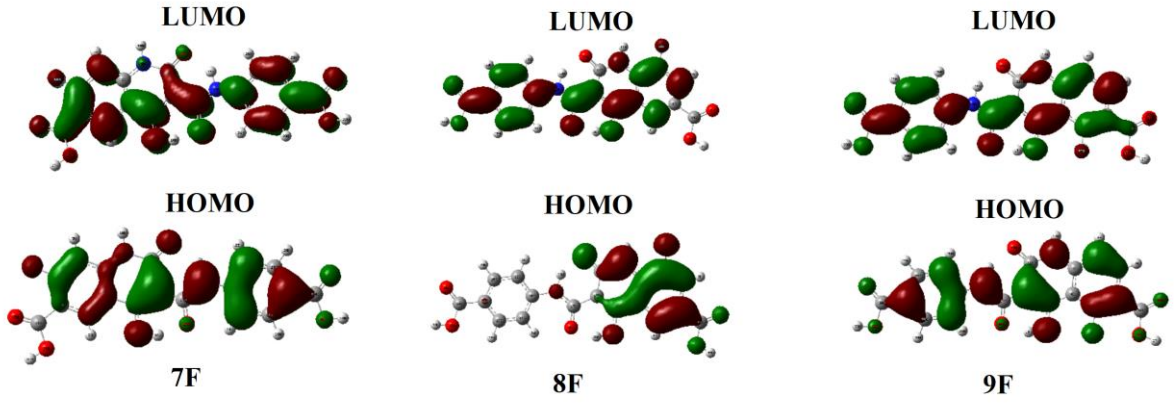

Fig. 4A. HOMO-LUMO plots of CPCHODQ6C with Fluorine substitution

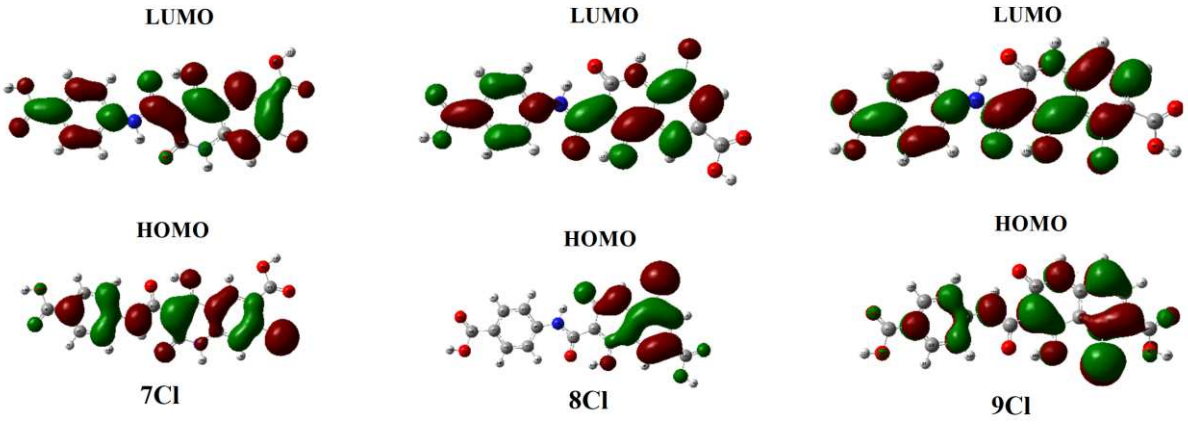

Fig. 4B. HOMO-LUMO plots of CPCHODQ6C with Chlorine substitution

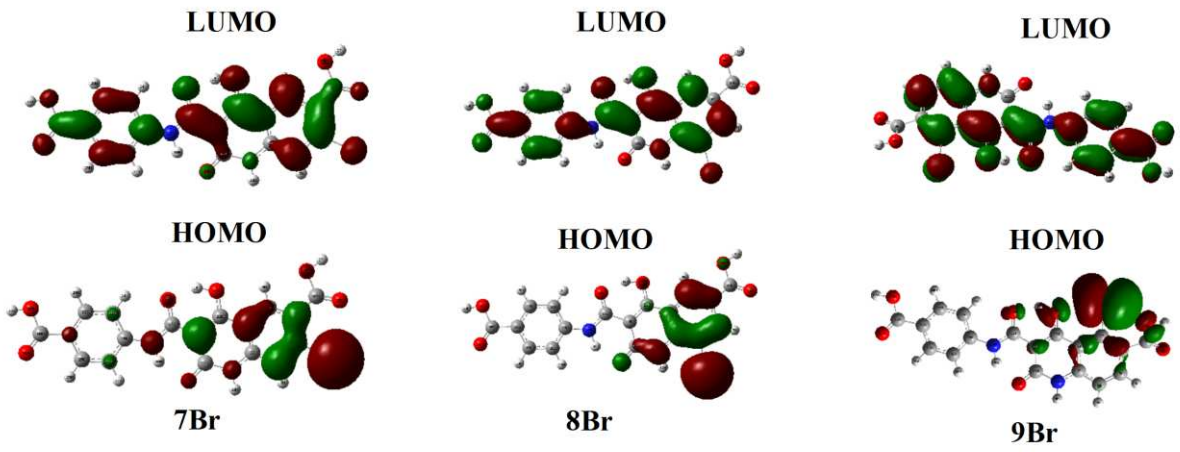

Fig. 4C. HOMO-LUMO plots of CPCHODQ6C with Bromine substitution

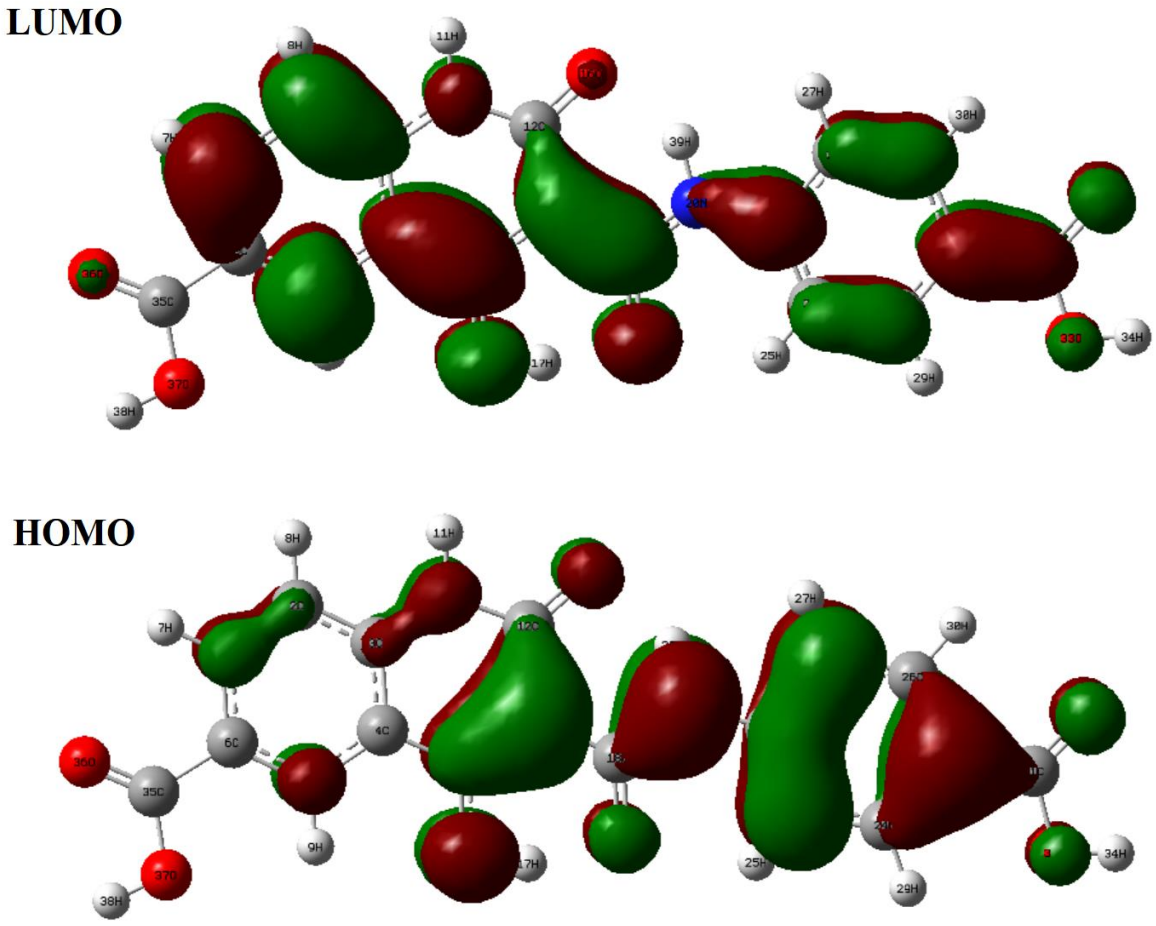

Fig. 4D. HOMO-LUMO plots of CPCHODQ6C

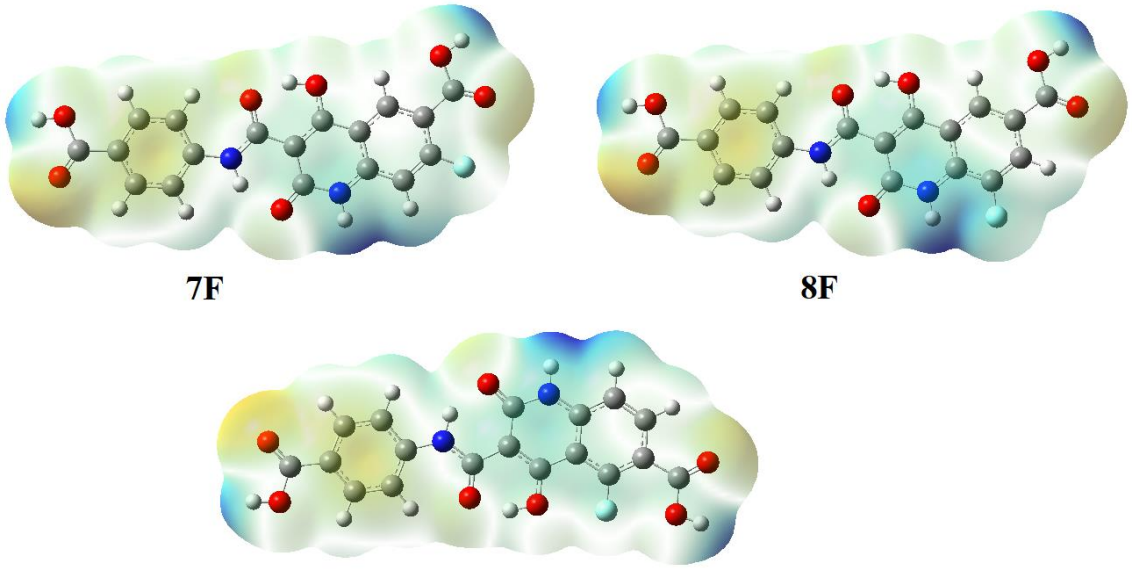

Fig. 5A. MEP plots of CPCHODQ6C with Fluorine substitution

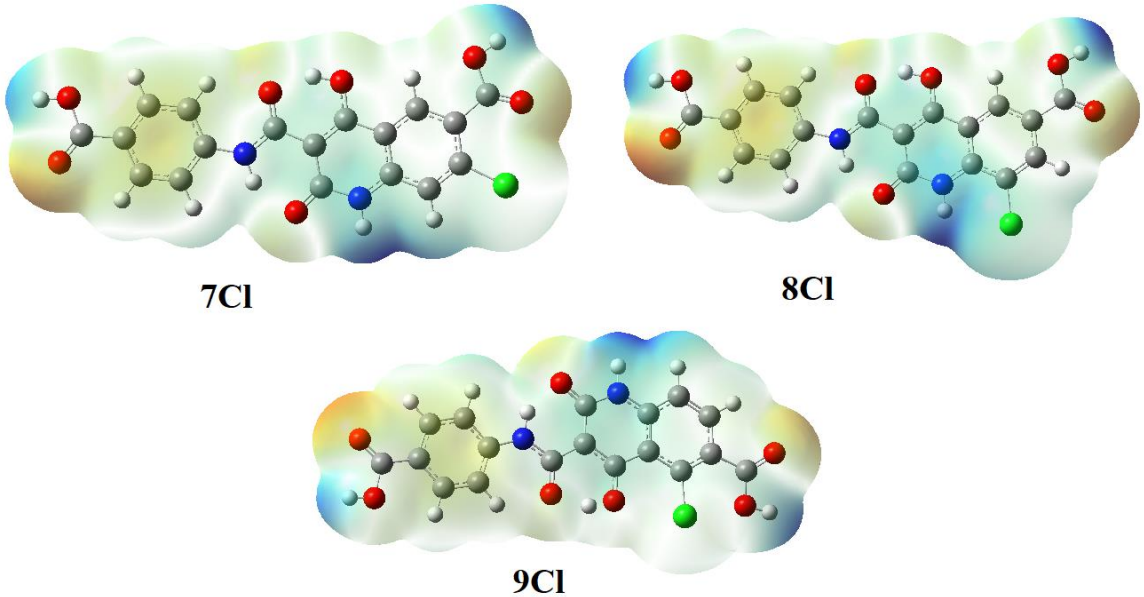

Fig. 5B. MEP plots of CPCHODQ6C with Chlorine substitution

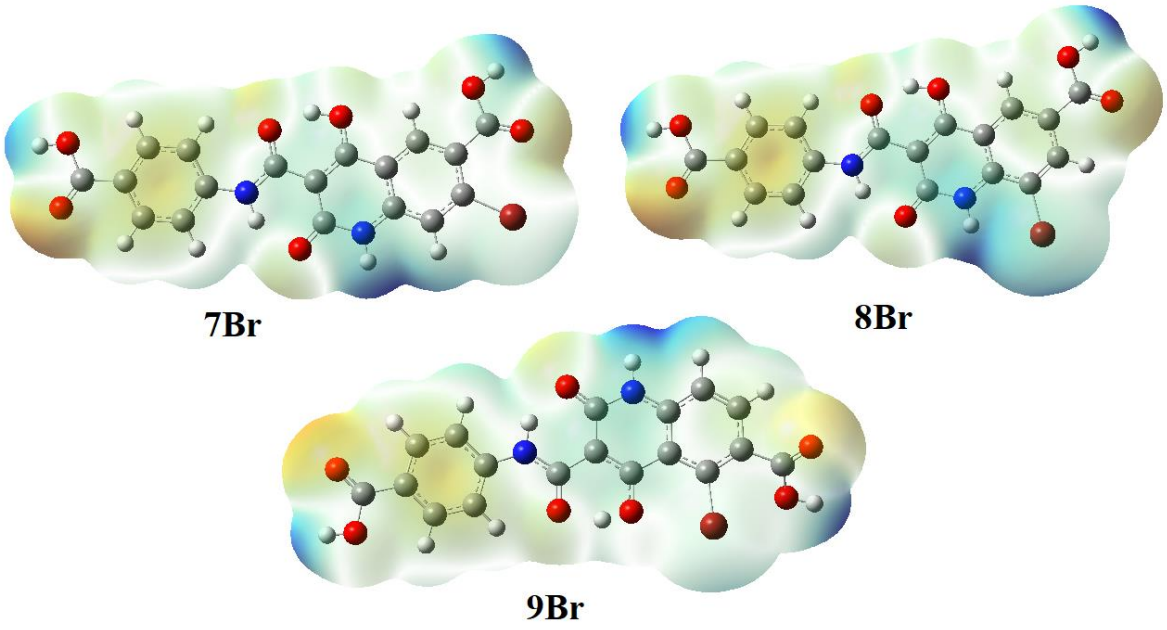

Fig. 5C. MEP plots of CPCHODQ6C with Bromine substitution

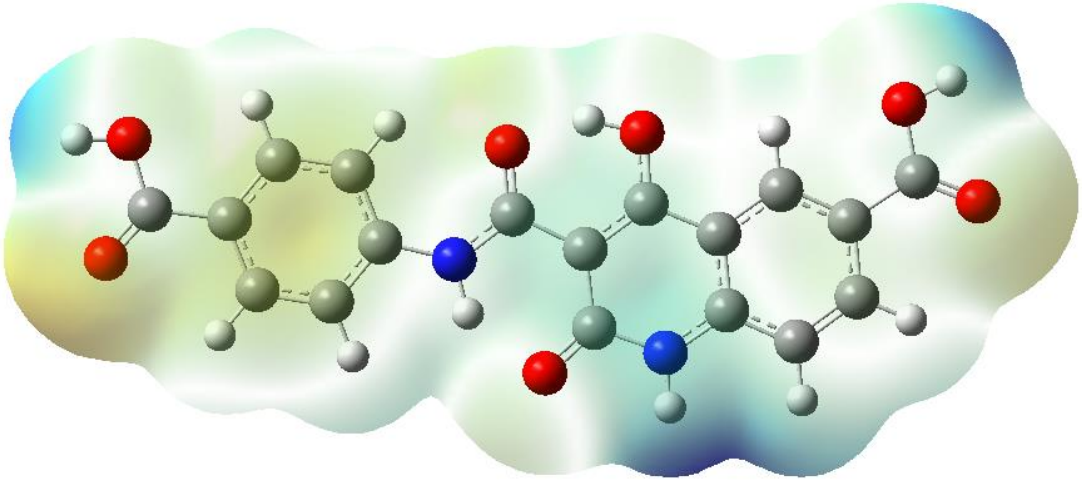

Fig. 5D. MEP plot of CPCHODQ6C

ALIE

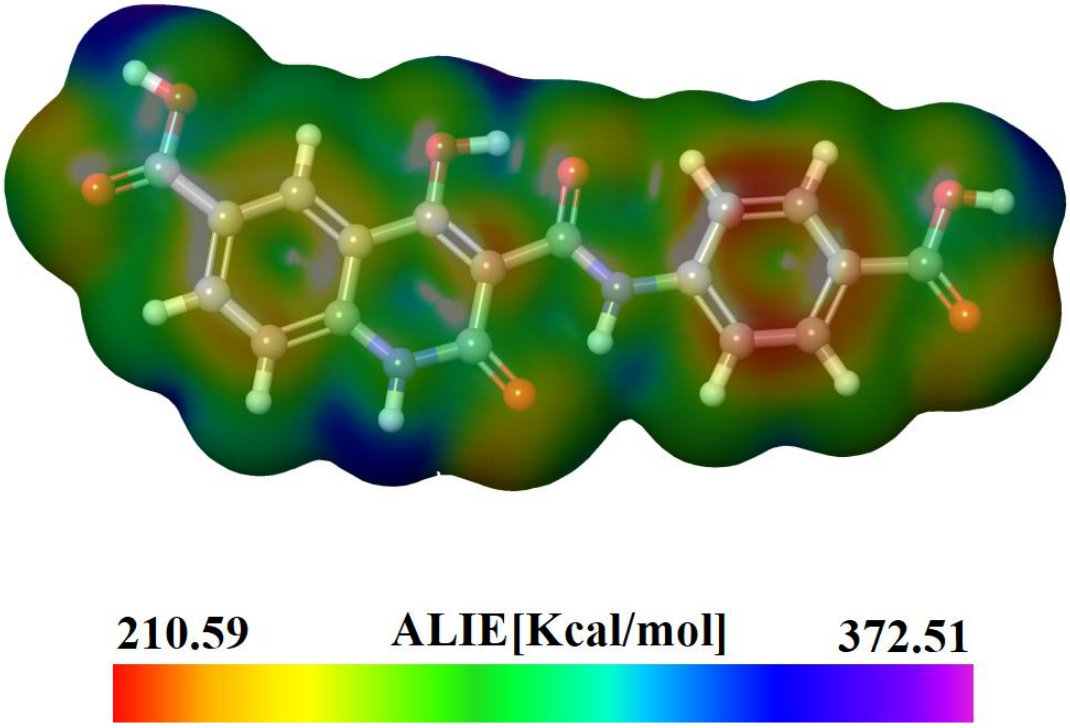

Fig. 6. ALIE surface of CPCHODQ6C

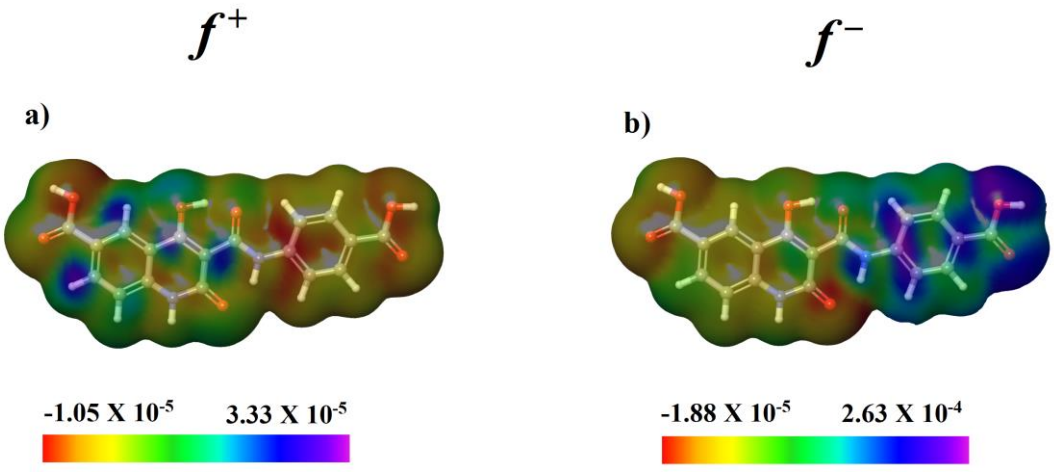

Fig. 7. Fukui functions a) f^+ and b) f^- of the CPCHODQ6C

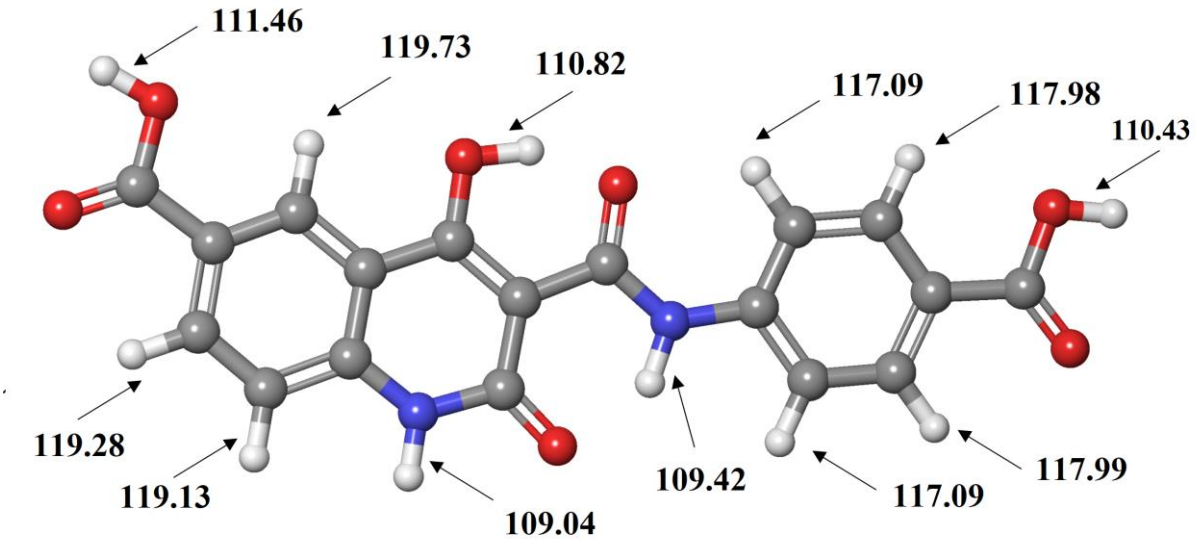

Fig. 8. BDEs of all single acyclic bonds of CPCHODQ6C

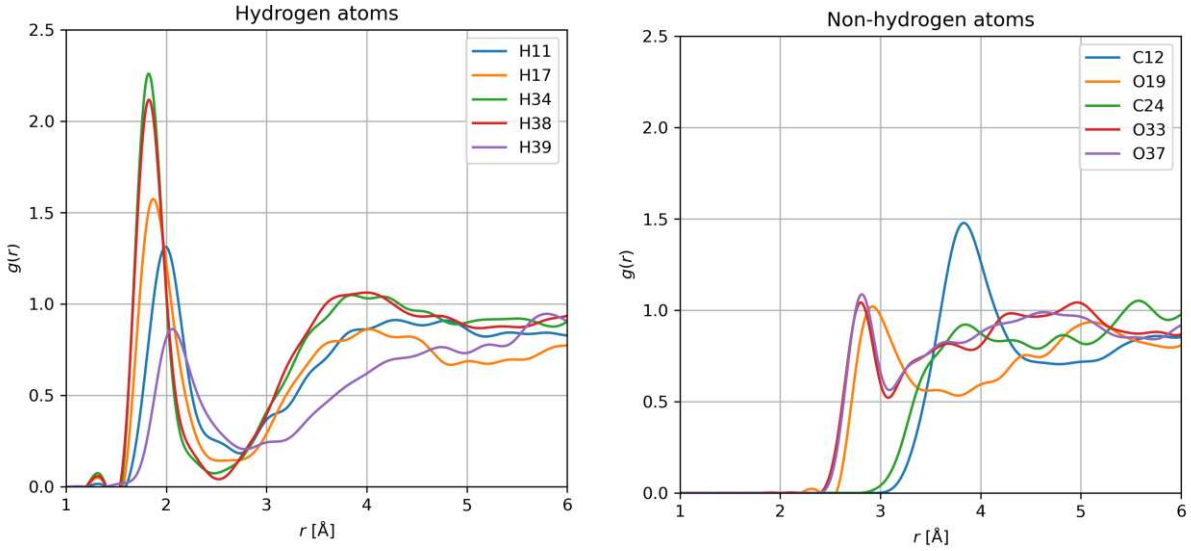

Fig. 9. RDFs of CPCHODQ6C atoms with significant interactions with water molecules

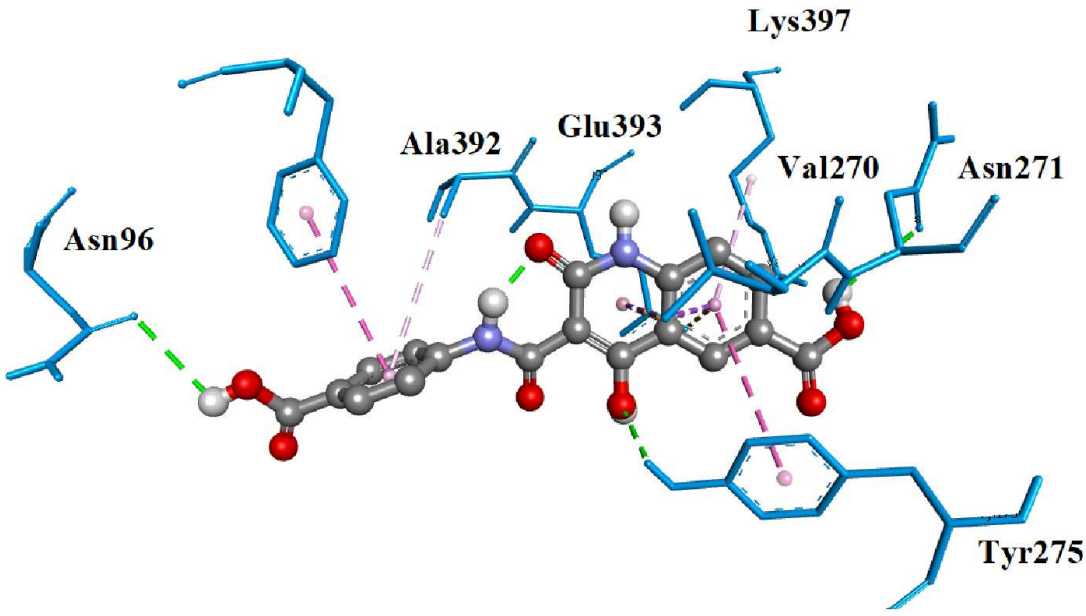

Fig. 10. Interactive plots of amino acids of the receptor with the ligand

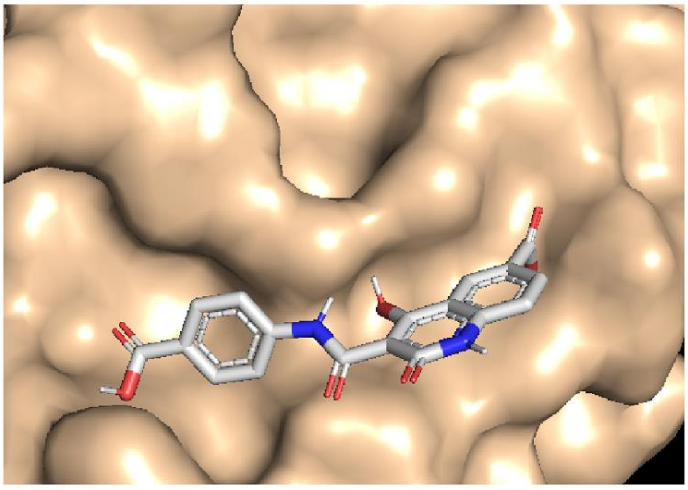

Fig. 11. The docked ligand of CPCHODQ6C at the active site of receptor

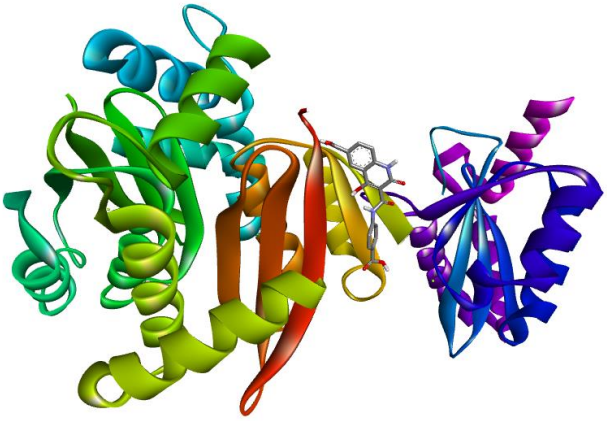

Fig. 12. The docked ligand embedded in the catalytic site of cytochrome BC1 complex

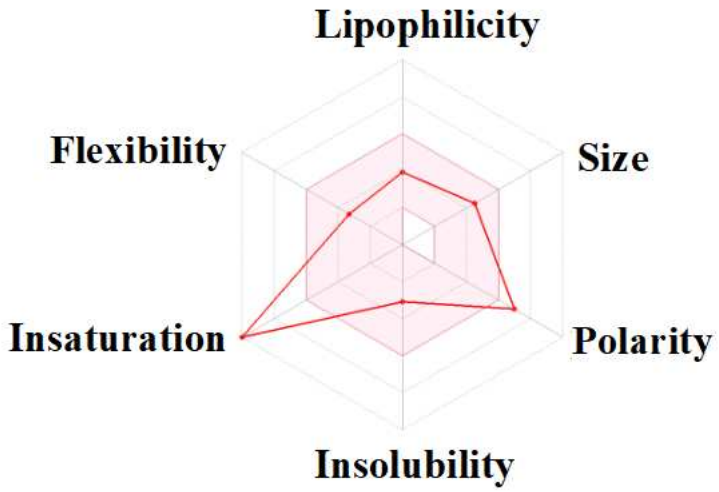

Fig. 13. The bioavailability radar of CPCHODQ6C

Table 1

Optimized Geometrical parameters of 3-[(4-carboxyphenyl) carbamoyl] -4-hydroxy-2-oxo-1, 2-dihydroquinoline-6-carboxylic acid.

Bond length (Å)		Bond angle (°)		Dihedral angle (°)	
C_1-C_2	1.3824	C_2-C_1-C_6	120.9	C_6-C_1-C_2-C_3	-0.0
C_1-C_6	1.4113	C_2-C_1-H_7	120.8	C_2-C_1-C_6-C_5	-0.0
C_1-H_7	1.0863	C_1-C_2-C_3	119.6	C_2-C_1-C_6-C_{35}	180.0
C_2-C_3	1.4084	C_1-C_2-H_8	120.7	C_1-C_2-C_3-C_4	0.0
C_2-H_8	1.0880	C_6-C_1-H_7	118.3	C_1-C_2-C_3-N_{10}	180.0
C_3-C_4	1.4130	C_1-C_6-C_5	119.6	C_2-C_3-C_4-C_5	0.0
C_3-N_{10}	1.3745	C_1-C_6-C_{35}	117.8	C_2-C_3-C_4-C_{13}	-180.0
C_4-C_5	1.4045	C_3-C_2-H_8	119.7	N_{10}-C_3-C_4-C_5	-180.0
C_4-C_{13}	1.4498	C_2-C_3-C_4	120.1	N_{10}-C_3-C_4-C_{13}	0.0
C_5-C_6	1.3916	C_2-C_3-N_{10}	121.3	C_2-C_3-N_{10}-C_{12}	-180.0
C_5-H_9	1.0841	C_4-C_3-N_{10}	118.6	C_4-C_3-N_{10}-C_{12}	0.0
C_6-C_{35}	1.4849	C_3-C_4-C_5	119.5	C_3-C_4-C_5-C_6	-0.0
N_{10}-H_{11}	1.0127	C_3-C_4-C_{13}	118.4	C_{13}-C_4-C_5-C_6	180.0
N_{10}-C_{12}	1.3914	C_3-N_{10}-H_{11}	119.9	C_3-C_4-C_{13}-C_{14}	-0.0
C_{12}-C_{14}	1.4579	C_3-N_{10}-C_{12}	126.0	C_3-C_4-C_{13}-O_{15}	-180.0
C_{12}-O_{16}	1.2374	C_5-C_4-C_{13}	122.1	C_5-C_4-C_{13}-C_{14}	180.0
C_{13}-C_{14}	1.3989	C_4-C_5-C_6	120.3	C_5-C_4-C_{13}-O_{15}	-0.0
C_{13}-O_{15}	1.3198	C_4-C_5-H_9	119.0	C_4-C_5-C_6-C_1	0.0
C_{14}-C_{18}	1.4854	C_4-C_{13}-C_{14}	121.2	C_4-C_5-C_6-C_{35}	-180.0
O_{15}-H_{17}	1.0122	C_4-C_{13}-O_{15}	115.9	C_1-C_6-C_{35}-O_{36}	0.0
O_{16}-H_{39}	1.7992	C_6-C_5-H_9	120.7	C_1-C_6-C_{35}-O_{37}	180.0
H_{17}-O_{19}	1.5785	C_5-C_6-C_{35}	122.5	C_5-C_6-C_{35}-O_{36}	-180.0
C_{18}-O_{19}	1.2507	C_6-C_{35}-O_{36}	124.7	C_5-C_6-C_{35}-O_{37}	-0.0
C_{18}-N_{20}	1.3596	C_6-C_{35}-O_{37}	113.0	C_3-N_{10}-C_{12}-C_{14}	-0.0
N_{20}-C_{21}	1.4047	H_{11}-N_{10}-C_{12}	114.0	C_3-N_{10}-C_{12}-O_{16}	180.0
N_{20}-H_{39}	1.0244	N_{10}-C_{12}-C_{14}	116.0	N_{10}-C_{12}-C_{14}-C_{13}	0.0
C_{21}-C_{22}	1.4068	N_{10}-C_{12}-O_{16}	118.0	N_{10}-C_{12}-C_{14}-C_{18}	180.0
C_{21}-C_{23}	1.4092	C_{14}-C_{12}-O_{16}	126.0	O_{16}-C_{12}-C_{14}-C_{13}	-180.0
C_{22}-C_{24}	1.3924	C_{12}-C_{14}-C_{13}	119.8	O_{16}-C_{12}-C_{14}-C_{18}	0.0
C_{22}-H_{25}	1.0814	C_{12}-C_{14}-C_{18}	122.1	C_4-C_{13}-C_{14}-C_{12}	-0.0
C_{23}-C_{26}	1.3864	C_{12}-C_{16}-H_{39}	99.6	C_4-C_{13}-C_{14}-C_{18}	-180.0
C_{23}-H_{27}	1.0896	C_{14}-C_{13}-O_{15}	123.0	O_{15}-C_{13}-C_{14}-C_{12}	180.0
C_{24}-C_{28}	1.4017	C_{13}-C_{14}-C_{18}	118.1	O_{15}-C_{13}-C_{14}-C_{18}	0.0
C_{24}-H_{29}	1.0859	C_{13}-O_{15}-H_{17}	106.1	C_{12}-C_{14}-C_{18}-O_{19}	180.0
C_{26}-C_{28}	1.4030	C_{14}-C_{18}-O_{19}	120.2	C_{12}-C_{14}-C_{18}-N_{20}	0.0
C_{26}-H_{30}	1.0863	C_{14}-C_{18}-N_{20}	116.8	C_{13}-C_{14}-C_{18}-O_{19}	0.0
C_{28}-C_{31}	1.4815	O_{15}-H_{17}-O_{19}	149.6	C_{13}-C_{14}-C_{18}-N_{20}	180.0
C_{31}-O_{32}	1.2132	O_{19}-C_{18}-N_{20}	123.0	C_{14}-C_{18}-N_{20}-C_{21}	-180.0
C_{31}-O_{33}	1.3596	C_{18}-O_{19}-H_{17}	103.1	O_{19}-C_{18}-N_{20}-C_{21}	0.0
O_{33}-H_{34}	0.9720	C_{18}-N_{20}-C_{21}	129.2	C_{18}-N_{20}-C_{21}-C_{22}	-0.0
C_{35}-O_{36}	1.2120	C_{18}-N_{20}-H_{39}	113.5	C_{18}-N_{20}-C_{21}-C_{23}	180.0
C_{35}-O_{37}	1.3554	C_{21}-N_{20}-H_{39}	117.3	N_{20}-C_{21}-C_{22}-C_{24}	-180.0
O_{37}-H_{38}	0.9722	N_{20}-C_{21}-C_{22}	124.3	C_{23}-C_{21}-C_{22}-C_{24}	0.0
		N_{20}-C_{21}-C_{23}	116.3	N_{20}-C_{21}-C_{23}-C_{26}	180.0

		N_{20}-H_{39}-O_{16}	141.9	C_{22}-C_{21}-C_{23}-C_{26}	-0.0
		C_{22}-C_{21}-C_{23}	119.4	C_{21}-C_{22}-C_{24}-C_{28}	0.0
		C_{21}-C_{22}-C_{24}	119.5	C_{21}-C_{23}-C_{26}-C_{28}	0.0
		C_{21}-C_{22}-H_{25}	119.7	C_{22}-C_{24}-C_{28}-C_{26}	-0.0
		C_{21}-C_{23}-C_{26}	120.5	C_{22}-C_{24}-C_{28}-C_{31}	180.0
		C_{21}-C_{23}-H_{27}	119.5	C_{23}-C_{26}-C_{28}-C_{24}	0.0
		C_{24}-C_{22}-H_{25}	120.8	C_{23}-C_{26}-C_{28}-C_{31}	-180.0
		C_{22}-C_{24}-C_{28}	121.2	C_{24}-C_{28}-C_{31}-O_{32}	180.0
		C_{22}-C_{24}-H_{29}	119.4	C_{24}-C_{28}-C_{31}-O_{33}	-0.0
		C_{26}-C_{23}-H_{27}	120.0	C_{26}-C_{28}-C_{31}-O_{32}	0.0
		C_{23}-C_{26}-C_{28}	120.4	C_{26}-C_{28}-C_{31}-O_{33}	180.0
		C_{23}-C_{26}-H_{30}	120.8		
		C_{28}-C_{24}-H_{29}	119.5		
		C_{24}-C_{28}-C_{26}	119.1		
		C_{24}-C_{28}-C_{31}	122.8		
		C_{28}-C_{26}-H_{30}	118.8		
		C_{26}-C_{28}-C_{31}	118.2		
		C_{28}-C_{31}-O_{32}	125.2		
		C_{28}-C_{31}-O_{33}	113.1		
		O_{32}-C_{31}-O_{33}	121.7		
		C_{31}-O_{33}-H_{34}	105.8		
		O_{36}-C_{35}-O_{37}	122.3		
		C_{35}-O_{37}-H_{38}	106.2		

Table 3

HOMO, LUMO and Chemical descriptors of CPCHODQ6C with halogen substitutions

	E_{HOMO}(LBS)	E_{LUMO}(LBS)	I = $-E_{HOMO}$	A = $-E_{LUMO}$	Gap	η	μ	ω
CPCHODQ6C	-8.482	-5.325	8.540	5.894	2.646	1.323	-7.217	19.684
7F	-8.423	-5.172	8..481	5.730	2.751	1.376	-7.106	18.349
8F	-8.276	-5.182	8.334	5.741	2.593	1.297	-7.038	19.095
9F	-8.404	-5.151	8.462	5.708	2.754	1.377	-7.085	18.227
7Cl	-8.105	-5.176	8.163	5.734	2.429	1.215	-6.949	19.872
8Cl	-7.885	-4.622	7.943	5.140	2.803	1.402	-6.542	15.263
9Cl	-8.039	-5.140	8.097	5.696	2.401	1.205	-6.897	19.738
7Br	-8.461	-5.288	8.519	5.854	2.665	1.333	-7.187	19.375
8Br	-8.484	-5.298	8.542	5.865	2.677	1.339	-7.196	19.336
9Br	-8.427	-5.283	8.485	5.849	2.636	1.318	-7.167	19.486

LBS=Larger Basis Set

Table 4

NBO result showing the formation of Lewis and non-Lewis orbitals

Bond (A-B)	ED/Energy	EDA%	EDB%	NBO	S%	P%
σC_1-C_2	0.98856	49.65	50.35	0.7046($sp^{1.79}$)C	35.80	64.20
-	-0.73127	-	-	+0.7096($sp^{1.75}$)C	36.32	63.68
πC_1-C_2	0.84908	45.37	54.63	0.6736($sp^{1.00}$)C	0.00	100.0
-	-0.28780	-	-	+0.7391($sp^{1.00}$)C	0.00	100.0
σC_1-C_6	0.98652	49.22	50.78	0.7016($sp^{1.88}$)C	34.78	65.22
-	-0.71144	-	-	+0.7126($sp^{1.93}$)C	34.11	65.89
σC_2-C_3	0.98554	48.51	51.49	0.6965($sp^{1.90}$)C	34.43	65.57
-	-0.73032	-	-	+0.7176($sp^{1.77}$)C	36.06	63.94
σC_3-C_4	0.98180	49.95	50.05	0.7068($sp^{1.81}$)C	35.65	64.35
-	-0.72658	-	-	+0.7074($sp^{2.04}$)C	32.91	67.09
σC_3-N_{10}	0.99237	38.03	61.97	0.6167($sp^{2.55}$)C	28.14	71.86
-	-0.85958	-	-	+0.7872($sp^{1.62}$)N	38.17	61.83
σC_4-C_5	0.98465	51.42	48.58	0.7171($sp^{1.84}$)C	35.15	64.85
-	-0.71830	-	-	+0.6970($sp^{1.88}$)C	34.72	65.28
σC_4-C_{13}	0.98382	50.54	49.46	0.7109($sp^{2.13}$)C	31.90	68.10
-	-0.71446	-	-	+0.7033($sp^{1.82}$)C	35.45	64.55
σC_5-C_6	0.98730	49.44	50.56	0.7031($sp^{1.82}$)C	35.41	64.59
-	-0.72601	-	-	+0.7110($sp^{1.79}$)C	35.88	64.12
πC_5-C_6	0.82480	42.74	57.26	0.6538($sp^{1.00}$)C	0.00	100.0
-	-0.28108	-	-	+0.7567($sp^{1.00}$)C	0.00	100.0
σC_6-C_{35}	0.98528	51.82	48.18	0.7199($sp^{2.34}$)C	29.96	70.04
-	-0.70075	-	-	+0.6941($sp^{1.49}$)C	40.15	59.85
σN_{10}-C_{12}	0.99174	63.95	36.05	0.7997($sp^{1.85}$)N	35.15	64.85
-	-0.82886	-	-	+ 0.6004($sp^{2.44}$)C	29.03	70.97
σC_{12}-C_{14}	0.98436	48.15	51.85	0.6939($sp^{1.62}$)C	38.21	61.79
-	-0.70828	-	-	+0.7201($sp^{2.03}$)C	33.05	66.95
σC_{12}-O_{16}	0.99437	35.12	64.88	0.5926($sp^{2.05}$)C	32.83	67.17
-	-1.01364	-	-	+0.8055($sp^{1.87}$)O	34.90	65.10
πC_{12}-O_{16}	0.98730	30.20	69.80	0.5495($sp^{99.99}$)C	0.00	100.0
-	-0.37506	-	-	+0.8355($sp^{1.00}$)O	0.01	99.99
σC_{13}-C_{14}	0.98751	49.53	50.47	0.7038($sp^{1.63}$)C	38.09	61.95
-	-0.75255	-	-	+0.7104($sp^{1.87}$)C	34.88	65.12
πC_{13}-C_{14}	0.84461	38.75	61.25	0.6225($sp^{1.00}$)C	0.00	100.0
-	-0.29939	-	-	+0.7826($sp^{1.00}$)C	0.00	100.0
σC_{13}-O_{15}	0.99445	33.10	66.90	0.5753($sp^{2.78}$)C	26.48	73.52
-	-0.93982	-	-	+0.8179($sp^{2.30}$)O	30.31	69.69
σC_{14}-C_{18}	0.98111	51.18	48.82	0.7154($sp^{2.12}$)C	32.04	67.96
-	-0.70381	-	-	+0.6987($sp^{1.66}$)C	37.58	62.42
σC_{18}-O_{19}	0.99269	32.35	67.65	0.5688($sp^{2.33}$)C	30.05	69.95
-	-0.82174	-	-	+0.8225($sp^{2.08}$)O	32.43	67.57
πC_{18}-O_{19}	0.97381	31.11	68.89	0.5577($sp^{99.99}$)C	0.42	99.58
-	-0.53501	-	-	+0.8300($sp^{99.99}$)O	0.79	99.21
σC_{18}-N_{20}	0.99039	40.13	59.87	0.6335($sp^{2.12}$)C	32.03	67.97
-	-0.83505	-	-	+0.7737($sp^{1.95}$)N	33.85	66.15
σN_{20}-C_{21}	0.98948	59.54	40.46	0.7716($sp^{1.61}$)N	38.38	61.26
-	-0.85498	-	-	+0.6361($sp^{2.36}$)C	29.73	70.27

σC_{21}-C_{22} -	0.98732 -0.70552	51.04 -	48.96 -	0.7144($sp^{1.81}$)C +0.6997($sp^{1.96}$)C	35.65 33.78	64.35 66.22
σC_{21}-C_{23} -	0.98568 -0.69940	51.52 -	48.48 -	0.7177($sp^{1.90}$)C +0.6963($sp^{1.94}$)C	34.54 34.03	65.46 65.97
σC_{22}-C_{24} -	0.98909 -0.72682	49.60 -	50.40 -	0.7042($sp^{1.74}$)C +0.7100($sp^{1.79}$)C	36.46 35.81	63.54 64.19
πC_{22}-C_{24} -	0.82033 -0.27619	40.71 -	59.29 -	0.6380($sp^{1.00}$)C +0.7700($sp^{1.00}$)C	0.00 100.0	0.00 100.0
σC_{23}-C_{26} -	0.98969 -0.72456	49.40 -	50.60 -	0.7029($sp^{1.76}$)C +0.7113($sp^{1.80}$)C	36.19 35.75	63.81 64.25
πC_{23}-C_{26} -	0.80982 -0.27298	39.89 -	60.11 -	0.6316($sp^{1.00}$)C +0.7753($sp^{1.00}$)C	0.00 100.0	0.00 100.0
σC_{24}-C_{28} -	0.98827 -0.71450	49.44 -	50.56 -	0.7031($sp^{1.91}$)C +0.7110($sp^{1.82}$)C	34.37 35.50	65.63 64.50
σC_{26}-C_{28} -	0.98708 -0.71181	49.41 -	50.59 -	0.7029($sp^{1.91}$)C +0.7112($sp^{1.88}$)C	34.36 34.75	65.64 65.25
σC_{28}-C_{31} -	0.98597 -0.70258	51.28 -	48.72 -	0.7161($sp^{2.37}$)C +0.6980($sp^{1.50}$)C	29.71 39.97	70.29 60.03
σC_{31}-O_{32} -	0.99631 -1.05946	34.18 -	65.82 -	0.5373($sp^{1.98}$)C +0.8434($sp^{1.80}$)O	0.00 0.00	100.0 100.0
πC_{31}-O_{32} -	0.98183 -0.39740	33.53 -	66.74 -	0.5847($sp^{1.00}$)C +0.8113($sp^{1.00}$)O	0.00 0.00	100.0 100.0
σC_{31}-O_{33} -	0.99564 -0.92044	30.75 -	69.25 -	0.5547($sp^{2.78}$)C +0.8321($sp^{2.17}$)O	26.48 31.57	73.52 68.43
σC_{35}-O_{36} -	0.99620 -1.05599	34.08 -	65.92 -	0.5838($sp^{1.98}$)C +0.8119($sp^{1.80}$)O	33.57 35.70	66.43 64.30
πC_{35}-O_{36} -	0.98967 -0.39675	30.73 -	69.27 -	0.5543($sp^{1.00}$)C +0.8323($sp^{1.00}$)O	0.00 0.00	100.0 100.0
σC_{35}-O_{37} -	0.99554 -0.91820	30.77 -	69.23 -	0.5547($sp^{2.79}$)C +0.8321($sp^{2.16}$)O	26.41 31.66	73.59 68.34
n_1N_{10} -	0.81511 -0.29998	- -	- -	$sp^{99.99}$ -	0.03 -	99.97 -
n_1O_{15} -	0.98581 -0.57445	- -	- -	$sp^{1.44}$ -	41.23 -	58.77 -
n_2O_{15} -	0.88442 -0.33551	- -	- -	$sp^{99.99}$ -	0.01 -	99.99 -
n_3O_{15} -	0.80785 -0.54637	- -	- -	$sp^{2.49}$ -	28.33 -	71.67 -
n_1O_{16} -	0.98710 -0.69479	- -	- -	$sp^{0.54}$ -	64.66 -	35.34 -
n_2O_{16} -	0.91141 -0.26540	- -	- -	$sp^{99.99}$ -	0.42 -	99.58 -
n_1O_{19} -	0.98252 -0.64215	- -	- -	$sp^{0.82}$ -	55.06 -	44.94 -
n_2O_{19} -	0.91962 -0.39219	- -	- -	$sp^{6.35}$ -	13.60 -	86.40 -
n_1N_{20} -	0.86698 -0.33229	- -	- -	$sp^{2.76}$ -	26.62 -	73.38 -

n_1O_{32} -	0.98829 -0.71587	- -	- -	$sp^{0.55}$ -	64.35 -	35.65 -
n_2O_{32} -	0.93126 -0.29119	- -	- -	$sp^{1.00}$ -	0.01 -	99.99 -
n_1O_{33} -	0.98979 -0.61362	- -	- -	$sp^{1.15}$ -	46.43 -	53.57 -
n_2O_{33} -	0.91343 -0.35262	- -	- -	$sp^{1.00}$ -	0.00 -	100.0 -
n_1O_{36} -	0.98819 -0.71428	- -	- -	$sp^{0.55}$ -	64.33 -	35.67 -
n_2O_{36} -	0.93154 -0.28884	- -	- -	$sp^{1.00}$ -	0.01 -	99.99 -
n_1O_{37} -	0.98969 -0.60952	- -	- -	$sp^{1.16}$ -	46.37 -	53.63 -
n_2O_{37} -	0.91664 -0.34980	- -	- -	$sp^{1.00}$ -	0.00 -	100.0 -

Table 5

Second-order perturbation theory analysis of Fock matrix in NBO basis corresponding to the intra molecular bonds of CPCHODQ6C

Donor(i)	type	ED/e	Acceptor(j)	Type	ED/e	E(2)[a]	E(j)-E(i)[b]	F(ij)[c]
C_5-C_6	σ	0.98733	$C_3$5-O_{36}	σ *	0.13399	1.25	1.20	0.049
-	π	0.82446	C_{35}-O_{36}	π*	0.13399	14.41	0.24	0.076
-	π	-	C_1-C_2	π*	0.12995	11.73	0.28	0.074
C_{13}-C_{14}	σ	0.98754	C_4-C_5	σ*	0.01001	1.84	1.26	0.061
-	σ	-	C_{18}-N_{20}	σ*	0.02628	1.55	1.16	0.054
-	π	0.84525	C_{12}-O_{16}	π*	0.00515	16.45	0.26	0.084
-	π	-	C_{18}-O_{19}	π*	0.13952	16.22	0.25	0.082
LPC_4	σ	0.54382	C_5-C_6	π*	0.15882	35.28	0.15	0.111
-	σ	-	C_{13}-C_{14}	π*	0.17309	37.81	0.13	0.106
LPN_{10}	σ	0.81494	C_{12}-O_{16}	π*	0.18382	27.67	0.26	0.108
LPO_{15}	σ	0.98597	C_{13}-C_{14}	σ*	0.01569	4.22	1.06	0.085
-	π	0.88385	C_{13}-C_{14}	π*	0.17309	22.49	0.32	0.110
LPO_{16}	σ	0.98828	N_{10}-C_{12}	σ*	0.03861	0.94	1.04	0.040
-	π	-	N_{10}-C_{12}	σ*	0.03861	11.50	0.62	0.107
-	π	-	C_{12}-C_{14}	σ*	0.02821	8.07	0.69	0.095
LPO_{19}	π	0.92775	C_{18}-N_{20}	σ*	0.02662	8.34	0.79	0.105
LPN_{20}	π	-	C_{18}-O_{19}	π*	0.98887	28.99	0.23	0.104
LPO_{32}	π	0.93175	C_{28}-C_{31}	σ*	0.98606	7.71	0.67	0.093
LPO_{32}	π	-	C_{31}-O_{33}	σ*	0.99564	16.26	0.54	0.119
LPO_{33}	σ	-	C_{31}-O_{32}	π*	0.99259	21.43	0.30	0.106
LPO_{36}	π	0.98819	C_{35}-O_{37}	σ*	0.99554	16.30	0.54	0.119
LPO_{37}	π	0.91664	C_{35}-O_{36}	π*	0.13399	21.44	0.31	0.105

Table 6
Polarizability values of CPCHODQ6C with halogen substitutions

	μ debye	α x10^{-23}esu	β x 10^{-30}esu	γ x 10^{-37}esu	MR = 1.333παN
CPCHODQ6C	3.7723	3.835	15.827	-37.219	96.680
7F	2.4881	3.852	14.266	-40.117	97.113
8F	3.3922	3.835	18.475	-38.524	96.684
9F	4.0094	3.844	15.433	-38.203	96.911
7Cl	2.2885	4.090	14.706	-43.982	96.684
8Cl	3.3286	4.014	19.209	-41.111	103.113
9Cl	4.2570	4.019	16.340	-40.007	101.323
7Br	2.6165	4.200	14.325	-46.681	105.886
8Br	3.4016	4.103	18.702	-42.842	103.441
9Br	4.3456	4.097	14.845	-41.671	103.289

Table 7.

Values of solubility parameters δ [$MPa^{1/2}$] for studied molecules and selected frequently used excipients

Molecules	δ [$MPa^{1/2}$]
CPCHODQ6C	27.411
PVP	18.515
Maltose	28.564
Sorbitol	32.425

Table 8

PASS prediction for the activity spectrum of CPCHODQ6C compound. Pa represents probability to be active and Pi represents probability to be inactive.

Pa	Pi	Activity
0.858	0.015	Ubiquinol-cytochrome-c reductase inhibitor
0.855	0.012	Methylenetetrahydrofolate reductase (NADPH) inhibitor
0.823	0.020	Testosterone 17beta-dehydrogenase (NADP+) inhibitor
0.777	0.017	Taurine dehydrogenase inhibitor
0.731	0.004	5 Hydroxytryptamine release inhibitor
0.732	0.014	Glutathione thiolesterase inhibitor
0.709	0.016	NADPH-cytochrome-c2 reductase inhibitor
0.705	0.015	2-Dehydropantoate 2-reductase inhibitor
0.700	0.012	Pterin deaminase inhibitor
0.690	0.005	N-methylhydantoinase (ATP-hydrolysing) inhibitor
0.711	0.026	Glutamate-5-semialdehyde dehydrogenase inhibitor
0.688	0.007	Aminobutyraldehyde dehydrogenase inhibitor
0.687	0.012	Kidney function stimulant
0.668	0.016	Fatty-acyl-CoA synthase inhibitor
0.673	0.029	Fusarinine-C ornithinesterase inhibitor
0.656	0.015	L-glutamate oxidase inhibitor
0.656	0.023	UDP-N-acetylglucosamine 4-epimerase inhibitor
0.641	0.008	Erythropoiesis stimulant
0.653	0.021	2-Hydroxyquinoline 8-monooxygenase inhibitor
0.639	0.007	Histamine release inhibitor
0.659	0.028	Ribulose-phosphate 3-epimerase inhibitor
0.646	0.017	Insulysin inhibitor
0.653	0.029	Dehydro-L-gulonate decarboxylase inhibitor

Table 9
The binding affinity values of different poses of the compound predicted by Autodock Vina.

Mode	Affinity (kcal/mol)	Distance from best mode (Å)	
-	-	RMSD l.b.	RMSD u.b.
1	-9.1	00.000	00.000
2	-8.7	23.021	25.648
3	-8.6	21.625	24.204
4	-8.5	04.709	06.627
5	-8.5	22.282	24.626
6	-8.2	15.464	16.890
7	-8.0	17.626	19.186
8	-8.0	02.659	10.111
9	-7.8	22.017	24.050

Table 10.

Drug-Likeness properties of the CPCHODQ6C compound

CPCHODQ6C	
MW	368.3 g/mol
nRot	5
HBA	7
HBD	5
TPSA	156.79$Å^2$
MlogP	0.96